Construction and Building Materials 369 (2023) 130591

Contents lists available at ScienceDirect

Construction and Building Materials

journal homepage: www.elsevier.com/locate/conbuildmat

Stochastic analysis for estimating track geometry degradation rates based on GPR and LiDAR data

Saeed Goodarzi [a,*], Hamed F. Kashani [b], Anahita Saeedi [c], Jimi Oke [a], Carlton L. Ho [a]

[a] Department of Civil and Environmental Engineering, University of Massachusetts Amherst, 28 Marston Hall, 130 Natural Resources Way, Amherst, MA 01003, United States

[b] Loram Technologies, Inc., P.O. Box 324, Williamsburg, MA 01096, United States

[c] Department of Biostatistics, School of Public Health & Health Sciences, University of Massachusetts Amherst, Amherst, MA 01003, United States

ARTICLE INFO

Keywords:
Probabilistic analysis
Large data
Preventive maintenance
Probability distribution fitting
Geometry data
Ground Penetrating Radar
LiDAR

ABSTRACT

The estimation of track degradation rate is a challenging step in scheduling preventive maintenance interventions due to its uncertain nature. To tackle this challenge, a large dataset of historic passenger track geometry data, between 2011 and 2021, integrated with Ground Penetrating Radar (GPR), and Light Detection And Ranging (LiDAR) data are investigated. Stochastic models are proposed for estimating the expected track degradation rates based on subsurface and drainage conditions of blocks and also a framework is proposed for automatically evaluating drainage conditions of track from LiDAR data. Results indicate that the probability of having high track degradation rates in highly fouled ballast condition can be 10 times more than in clean ballast condition. In addition, analyzing the effect of drainage conditions revealed that sections with poor drainage conditions are 30% more likely to have high track degradation rates than sections with moderate drainage conditions. The results of this study enhance scheduling geometry maintenance and provide reliable information for decision making on different types of maintenance such as Ballast Cleaning and ditching.

1. Introduction

Train dynamic loads lead to degradation of the track structure and result in a discrepancy between the actual track geometry and the intended design. The evolution of track deviations decreases the ride quality and might result in derailment in extreme cases. Properly maintaining geometry defects is required to ensure passengers' safety and network availability. The railway industry, same as many other industries, is also moving toward predictive maintenance to reduce corrective maintenance which can be very costly and can result in reducing track safety and increasing the potential of track closure [1–4]. To schedule preventive maintenance, railway companies should either predict the occurrence of defects in the future or predict the value of track degradation rate.

Many studies have been conducted on predicting the near-future occurrence of geometry defects [5–19]. In a recent research study, Goodarzi et al. [5] predicted the occurrence of yellow-tag defects in the next inspection using logistic regression and Gradient Boosting Machine. They considered geometry history, applied traffic in Million Gross Tonnes (MGT), class of track, and Ballast Fouling Index (BFI) as explanatory variables. Soleimanmeigouni et al. [6] found that kurtosis of longitudinal level is a good indicator for predicting isolated defects. Zarembski et al. [20] forecasted geometry degradation from BFI and fouling depth layer. Cardenas-Gallo et al. [14] predicted the evolution of yellow-tag defects to a certain level considering MGT, Class of track, and previous geometry data as input variables. They demonstrated that ensemble classifiers improve results of single classifiers in all types of geometry defects.

Predicting the occurrence of defects is ideal for short-term maintenance scheduling, as classification methods can accurately predict defects in the near future. The long-term scheduling of maintenance requires long-term degradation rate of track, which is affected by numerous factors. Stochastic and probabilistic models are appropriate for describing the expected track degradation rate due to its uncertain nature and inability to capture all contributing factors [4]. Vale and Lurdes [21] proposed stochastic models by fitting different probability distributions on track degradation rates. They divided data into different groups based on the class of track and time intervals of geometry

* Corresponding author.
E-mail addresses: sgoodarzitae@umass.edu (S. Goodarzi), hamed.f.kashani@loram.com (H.F. Kashani), asaeedi@umass.edu (A. Saeedi), jboke@umass.edu (J. Oke), ho@umass.edu (C.L. Ho).

https://doi.org/10.1016/j.conbuildmat.2023.130591
Received 21 September 2022; Received in revised form 25 January 2023; Accepted 29 January 2023
Available online 6 February 2023
0950-0618/

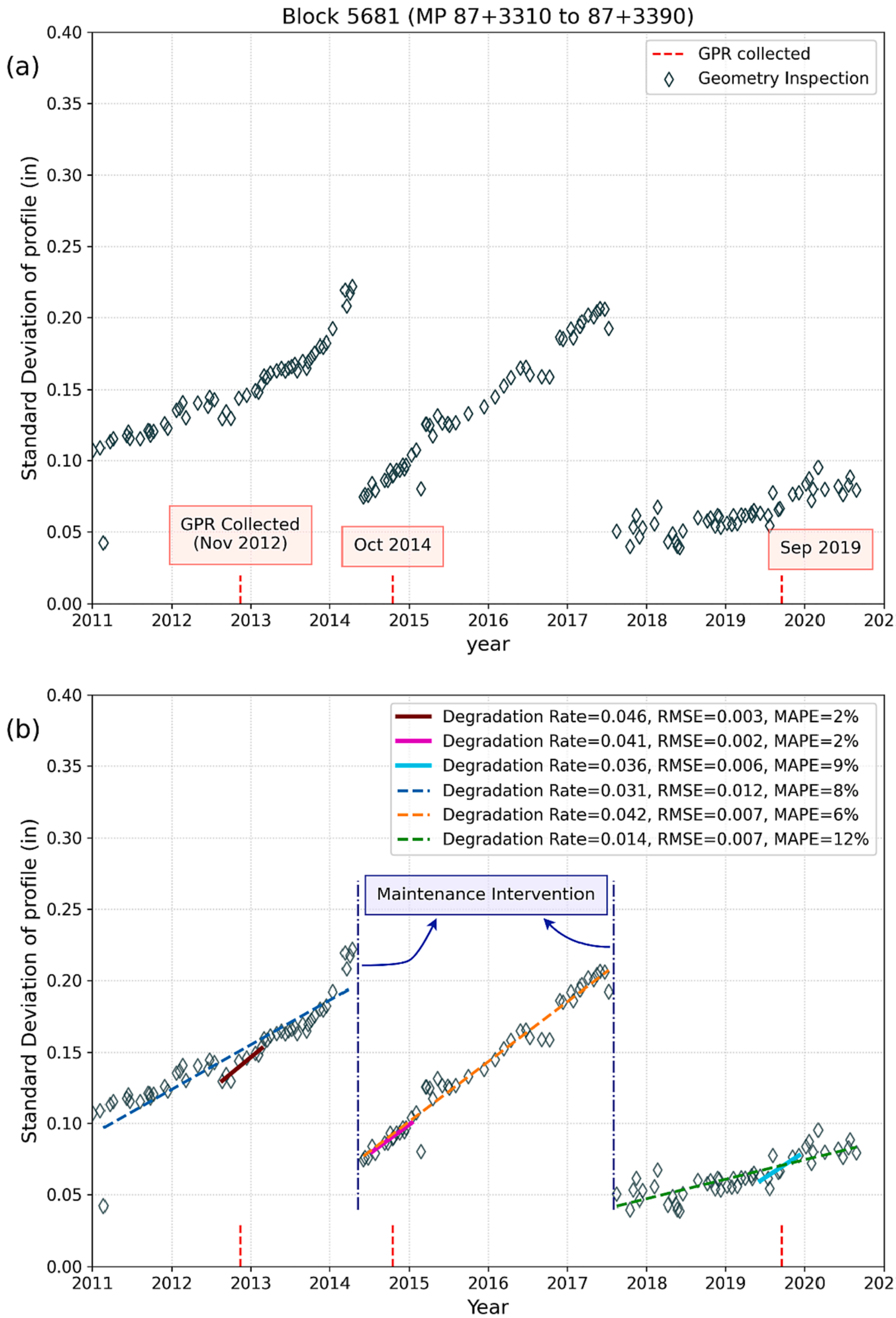

Fig. 1. An Example of studied profile Geometry data of a block (a) SD of profile for different geometry inspections vs time and dates of collecting GPR; (b) fitted linear regression models to calculate track degradation rates; solid and dotted lines represent short and long period degradation, respectively.

inspections. Audley and Andrews [22] investigated the detrimental effects of tamping on track degradation rates using probabilistic modeling.

The subsurface conditions of track have significant effects on track degradation rate. It has been shown in many laboratory studies that high amount of fouling in ballast layer reduces the layer strength and consequently increases track degradation rate [23–32]. Kashani et al. [23,24] used large scale trxial and box test to indicate that there is an inverse correlation between ballast fouling amount and ballast layer strength. This study indicated that in dry condition, increase in the amount of fouling particles in the ballast layer can locally increase the strength of the ballast due to improving its gradation, but introducing a small amount of moisture, which exists in real track, will reverse this correlation.

Because measuring the fouling index of the ballast layer needs actual sampling and lab testing, measuring ballast fouling for the entire length of track is infeasible. Thus, Non-Destructive Testing (NDT) methods such as Ground Penetrating Radar (GPR), which relies on wave propagation, are employed and calibrated for ballast fouling condition monitoring and evaluating other subsurface conditions such as moisture level and layer thicknesses. By using frequency spectrum analysis on GPR data, Ballast Fouling Index (BFI) can be determined [33–40]. Silvast et al. [41] validated the correlation between GPR interpolation and BFI by conducting multiple tests on different tracks. GPR data are collected by transmitting electromagnetic waves from antennas and recording the reflected waves from subsurface of track. Liu et al. [42] employed three antenna frequencies to investigate their effect on GPR calibration using full-scale track model. The difference between dielectric permittivity of materials is the key factor for interpolating GPR results [33]. In this study, the GPR interpolation determines subsurface conditions for left, center, and right sides of tracks similar to the previous paper [5].

The drainage condition of track is another factor that has a considerable impact on the track degradation rate as it determines the amount of remaining water in track after precipitation. Rohrman et al. [25] investigated the effect of water on ballast properties by using large-scale box tests. They indicated that additional water in track will significantly increase the track settlement under the applied load. The detrimental effects of water on strength of ballast are also shown by triaxial tests in another study performed by Kashani et al. [24]. Undrained water in the highly fouled ballast layer under the ties affects the strength properties of ballast and increase the track's rate of deterioration. Drainage of the track is the most important consideration in track design and maintenance [27]. Track must have good internal and external drainage, where internal drainage maximizes the flow of water out of the track and external drainage ensures that water is carried away from track [27]. Further, both internal drainage, defined by fouling conditions of the track, and external drainage, defined by Right-of-Way conditions, must work together. The external drainage conditions of the track can be evaluated by LiDAR (Light Detection And Ranging) data.

To collect LiDAR data, a laser scanner will be mounted on a hi-rail vehicle or a track maintenance car. The distance of surrounding objects, such as adjacent terrain can be determined from the reflection of laser pulses [43]. LiDAR has been widely used in the railway industry for various purposes [44–51]. LiDAR data was utilized to measure the ballast profile [52] and to determine the discrepancies in the ballast level compared to the designed track geometry, both in terms of deficit and excess [44]. Lan et al. [45] utilized LiDAR to investigate rockfall hazards on Canadian railway track. Zhangyu et al. [46] used a combination of LiDAR data and camera photos to detect small obstacles existing in front of trains. Arastounia [51] utilized LiDAR for recognizing different railroad infrastructure such as rails and catenary cables. LiDAR data have also been used for determining lateral irregularities, alignment and gauge variations [47].

Although many studies have been conducted on applications of LiDAR in railways, to date, no research has utilized LiDAR for evaluating drainage conditions of track. To address this gap, a novel framework is proposed in this study that automatically evaluates the lateral cross section and drainage condition of track using LiDAR data. In addition to drainage, the subsurface condition of track from GPR data is considered as another factor. The expected track degradation rate is estimated based on subsurface and external drainage conditions. The remainder of this study is organized as follows; Section 2 describes geometry data and methodologies for calculating track degradation rates. Section 3 describes categories for subsurface and drainage conditions of track. Section 4 presents stochastic models and details of fitting probability distributions. Section 5 provides the conclusions of this paper.

2. Track degradation rate

2.1. Geometry data

In the railway industry, track geometry data are regularly collected to detect problematic sections of the track, evaluate the rate of deterioration and finally schedule maintenance intervention. This is attributed to the fact that the safety of track is ensured by keeping geometry defects under certain thresholds specified in compliance manuals [53]. The cumulated large dataset over years provides a great opportunity for extracting valuable knowledge regarding the mechanical behavior of railway track.

In this study, the geometry data of a passenger revenue track with a cumulative length of 130 miles (209.2 km) consisting of Classes 6, 7, and 8 were used. It should be noted that the speed limit of Classes 6, 7, and 8 are 110 mph, 125 mph, and 160 mph respectively. One hundred and forty-six (146) geometry inspections that were conducted from 2011 to 2021 are analyzed in this study. The entire track is divided into blocks, each with a length of 80 ft (24.38 m). As geometry inspections provide data for every foot of track, there are 80 datapoints in each block. The 62-ft profile mid-chord offset channel is considered in this study since it is the best indicator of existence of subsurface problems according to the Federal Railroad Administration (FRA) manual [53].

2.2. Data preprocessing

The role of data preprocessing is essential in railway large datasets due to much noise and variations in the data, which is attributed to uncalibrated sensors, various weather conditions, and unaligned inspections. Although geometry cars employ GPS (Global Positioning System) for the geographical location of data, datasets from different inspections can be unaligned by a few feet or more. In this study, cross-correlation algorithm is used to find the amount of positional errors between the inspections. The measurements from different dates are shifted along each other based on the positional errors for data alignment [54].

The dynamic loads of trains in assets such as switches, under-grade bridges, and interlocking is higher than open tracks [55,56]. Therefore, the settlement and overall behavior of track at the asset locations are different from open tracks. To achieve accurate estimations of track degradation rate for open tracks, blocks with assets are removed from the dataset.

2.3. Calculating track degradation rate

Track degradation rate refers to the changes in geometry indices over time or traffic (MGT). Different geometry indices such as Standard Deviation (SD), Track Roughness, or Track Quality Index (TQI) are employed in the railway industry to represent the condition of tracks [54,57]. As SD has the best correlation with track settlement [54], this geometry index is employed in the current study. SD is the amount of variation of a set of geometry defects from the mean value of a block. Fig. 1 (a) shows the SD of profile vs time for an example block. As track degradation rate can be more accurately estimated based on subsurface conditions, it should be calculated around the dates of collecting GPR data. The GPR for this block is collected in Nov 2012, Oct 2014, and Sep 2019.

Two different methods are employed for calculating track degradation rate, namely, short period degradation and long period degradation. In short period degradation, geometry inspections that were three months before and after the date of collecting GPR are selected (e.g., geometry inspections from Aug 2012 to Feb 2013 are selected for GPR data in Nov 2012). Then, a linear regression model is fitted to the

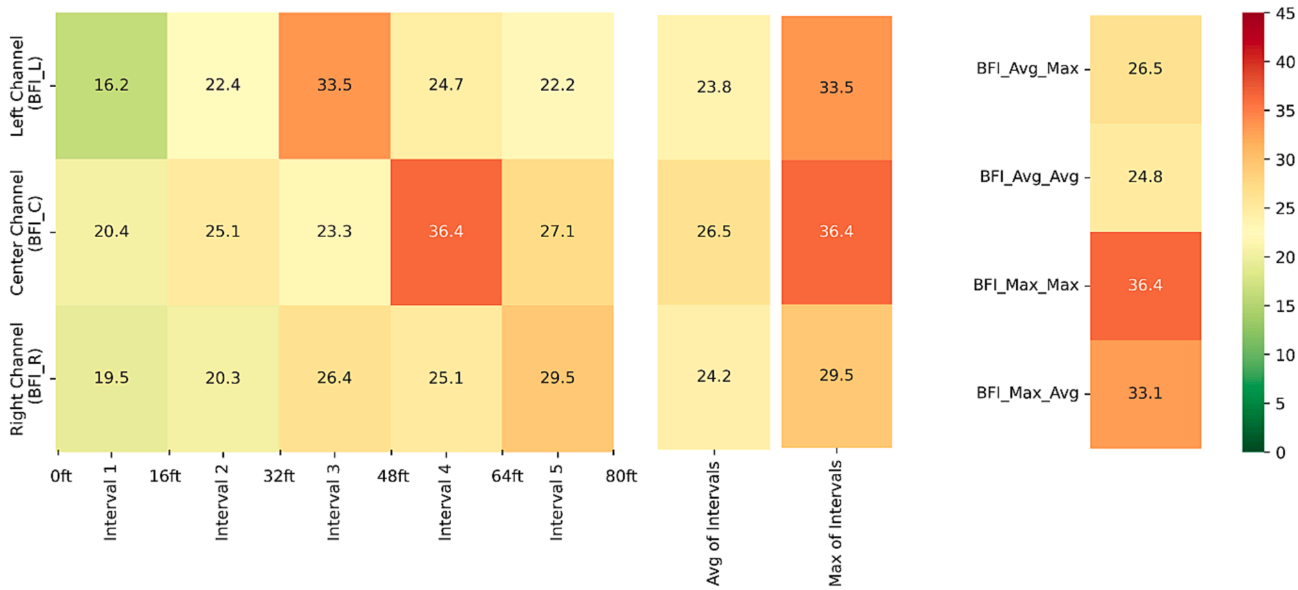

Fig. 2. The BFI data in a block as an example and summarizing approaches; the final value of BFI in a block highly depends on the summarizing approach.

selected inspections. The slope of the fitted line represents short period degradation at the date of collecting GPR (shown by solid lines in Fig. 1 b). In long period degradation method, detection of previous maintenance interventions is required to filter out the maintenance effects on geometry behavior. Correctly detecting previous maintenance interventions is a complex task due to high variations and noise in geometry data. To cope with these variations, a combination of 4 conditions is considered, which distinguishes the difference between the noise and reduction of SD due to maintenance interventions. These conditions and details are provided in the previous paper by the authors of this study [5]. After detecting previous maintenance, linear regression models are fitted to the inspections between two maintenance interventions (shown by dotted lines in Fig. 1 b). The slope of the fitted line that covers the date of collecting GPR represents long period degradation for that specific date. A comparison between the effectiveness of short and long period degradation and their correlation with BFI is presented in Section 3.1.

To ensure the reliability of fitted lines and in turn, calculated track degradation rates, performance metrics such as RMSE (Root Mean of Squared Error), MAPE (Mean of Absolute Percentage Error), and MAD (Mean of Absolute Deviation) are calculated. If the MAPE of a fitted line was higher than 15%, the calculated degradation rate was considered as unreliable observation and was removed from the dataset. It should be noted that only 12% of datapoints were recognized as unreliable observations.

$$RMSE = \sqrt{\frac{1}{N}\sum_{i=1}^{N}(A_i - P_i)^2}$$

$$MAPE = \frac{\sum_{i=1}^{N}|A_i - P_i|}{\sum_{i=1}^{N}A_i} \times 100$$

$$MAD = \frac{\sum_{i=1}^{N}|A_i - P_i|}{N}$$

where, A_i and P_i are the actual and predicted values of SD for ith observation, respectively. N is the number of inspections that are selected for fitting a linear regression model.

3. Categorizing the dataset

In stochastic analysis, dividing the entire dataset into subgroups based on their properties result in more accurate estimations [21]. This is attributed to the fact that smaller groups with similar properties are more likely to have similar behavior compared to the entire dataset. Choosing types of properties for categorizing the dataset is very important as it directly affects the accuracy of estimated output. Categorization should have the following two qualities: (i) it should be typical so that it can be used on other datasets; (ii) it should be effective so that it increases the accuracy of estimations. In this study, subsurface and drainage conditions of tracks are chosen for categorizing data as they have a significant impact on track degradation rate. The chosen categories are also typical and can be used for other passenger tracks with similar conditions. It should be noted that the class of track was another potential category. However, as revealed in the previous study [5], track degradation rate is relatively similar for Classes 6, 7, and 8. Thus, class of track was not an effective category and consequently was not considered in this paper.

3.1. Categorizing based on subsurface condition

Subsurface conditions of tracks can be determined from GPR inspections. Important properties such as BFI and ballast thickness can be extracted from interpolated GPR data [35,37,40,41]. In this study, BFI is chosen to represent subsurface condition as it is the most important feature that can be extracted from GPR data. As three antennas were employed for collecting GPR, BFI data are provided for three channels (i.e., center of track, left and right shoulders). The interval of BFI data along the track is 16 ft (4.88 m); therefore, there are 15 BFI values in each 80-ft (24.38-m) block as shown in Fig. 2. These values should be summarized into a single number (using averaging or maximizing) so that a representative number can be used for categorizing the dataset. The correlation between track degradation rate and different approaches for defining the representative BFI values in a block should be investigated to find the best representative for the block. These correlations provide valuable information for making the right solution for cleaning the track. For example, if track's degradation rate has a high correlation with the maximum of BFI values, the fouled ballast should be replaced with clean ballast even if BFI is high only in one interval (i.e.,

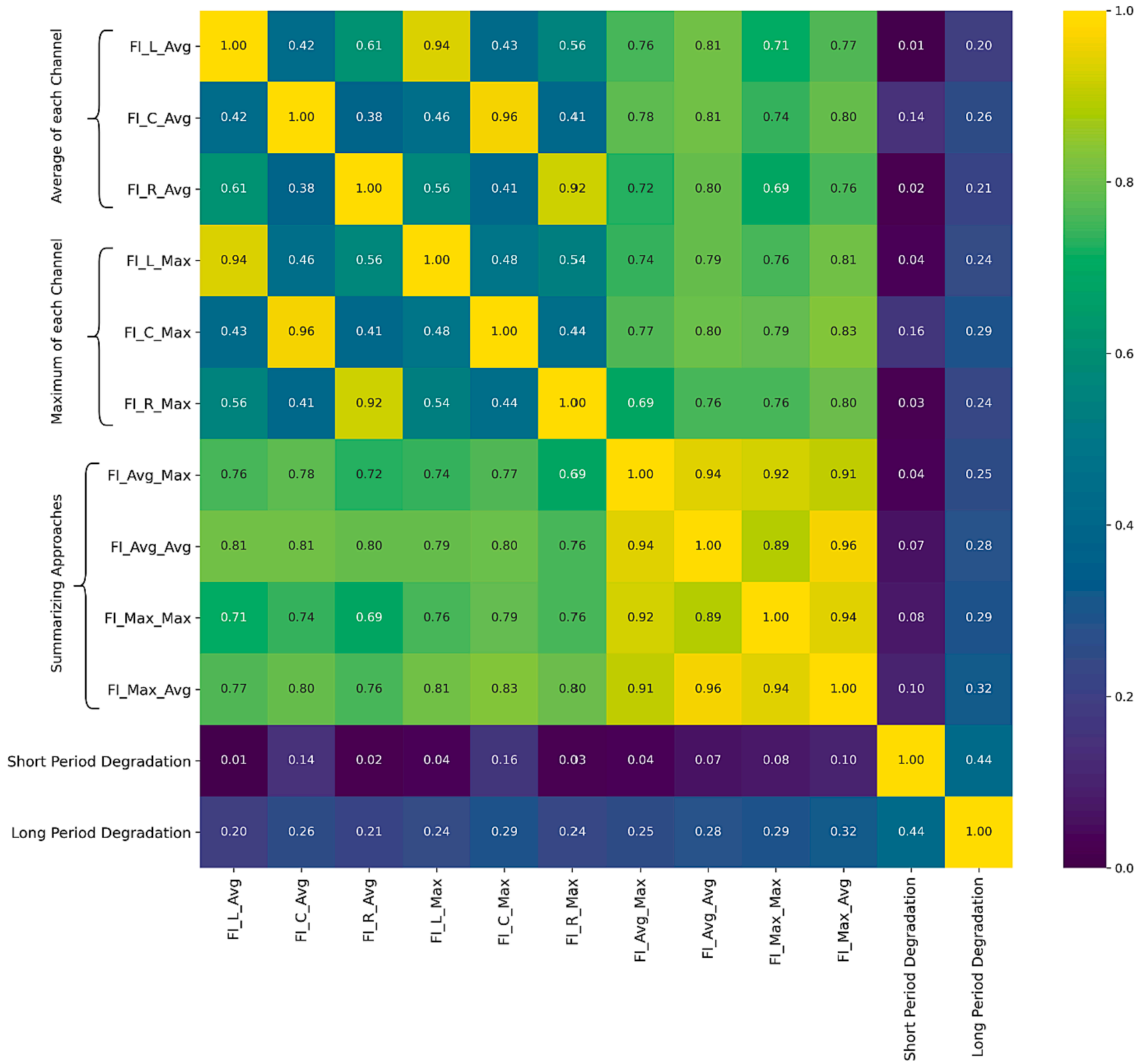

Fig. 3. The correlation plot using Pearson equation; The correlation between BFI data and long period degradation is higher than short period.

16 ft). On the other hand, if track degradation rate has a high correlation with the average of BFI values, the cleaning should be scheduled only for blocks that have high BFI in all intervals. Therefore, the summarizing approach to calculate the appropriate BFI representative has a significant impact on maintenance planning. The following approaches are employed for calculating the BFI representative value in a block (Fig. 2):

- BFI_Avg_Max: Calculates the average for each channel then considers the maximum value of three calculated averages
- BFI_Avg_Avg: Calculates the average for each channel then considers the average value of three calculated averages (i.e., overall average)
- BFI_Max_Max: Calculates the maximum value for each channel then considers the maximum value of three calculated maximums (i.e., overall maximum)
- BFI_Max_Avg: Calculates the maximum value for each channel then considers the average value of three calculated maximums

Fig. 3 shows the Pearson Correlation between different approaches for calculating BFI representative value and Track degradation rate. BFI has a higher correlation with long period degradation than with short period degradation regardless of BFI channel or summarizing approach. Thus, long period degradation can better represent track behavior. Among the three BFI channels, the center of track shows a better correlation with track degradation rate compared to the shoulders. This could be attributed to the center BFI having a more profound impact on the degradation rate due to the stress distribution of train dynamic loads. More precisely, stresses of train loads are higher in the center of track than in the shoulders. Thus, high BFI in the center of track causes more settlement and track degradation rate compared to the shoulders.

Table 1
Categorizing dataset based on subsurface condition of track.

Name of Category	BFI Limits	Description
G1	$5 \leq BFI < 15$	Clean Ballast
G2	$15 \leq BFI < 25$	Moderately Fouled Ballast
G3	$25 \leq BFI < 35$	Fouled Ballast
G4	$35 \leq BFI < 45$	Highly Fouled Ballast

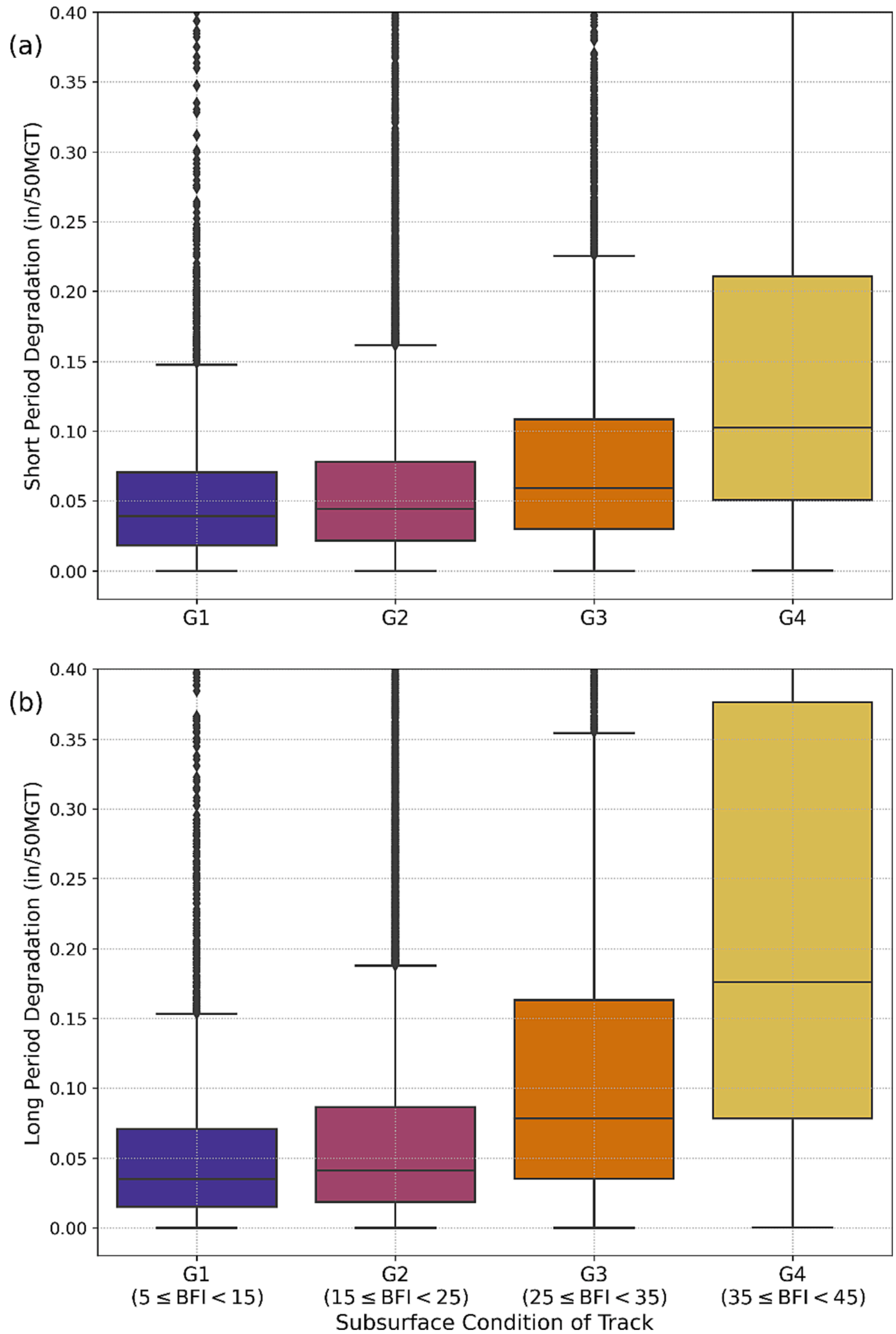

Fig. 4. Box plot of track degradation rate with respect to subsurface conditions; (a) short period degradation; (b) long period degradation.

Among the summarizing approaches, BFI_Max_Avg has the best correlation with track degradation rate. Thus, this approach is employed for calculating the final representative value of BFI for each block and categorizing the dataset based on subsurface conditions. The entire dataset is divided into four categories from clean ballast to highly fouled ballast as presented in Table 1.

Fig. 4 shows the box plot of track degradation rate with respect to subsurface categories. Track degradation rate increases with increasing fouling in ballast both for short period and long period methods of calculating degradation rate. However, the difference between categories of long period degradation is much higher than short period degradation, which indicates the superiority of this method to represent track behavior. Therefore, only long period degradation is employed for the rest of analysis in this paper to avoid presenting redundant results. It should be noted that the direct correlation between BFI and track settlement is observed in many laboratory studies [23–25,31,32].

3.2. Categorizing based on cross-section and drainage conditions

In addition to BFI, drainage conditions of track affect track degradation rates. If the external drainage of track has poor condition, the water from precipitations will remain in the track and results in high degradation rates. The negative effects of additional water in track are observed by box tests [23,25]. To investigate the drainage condition of track, the combination of ditch geometry and track cross-section derived from Lidar data are analyzed. For example, if track is on fill,

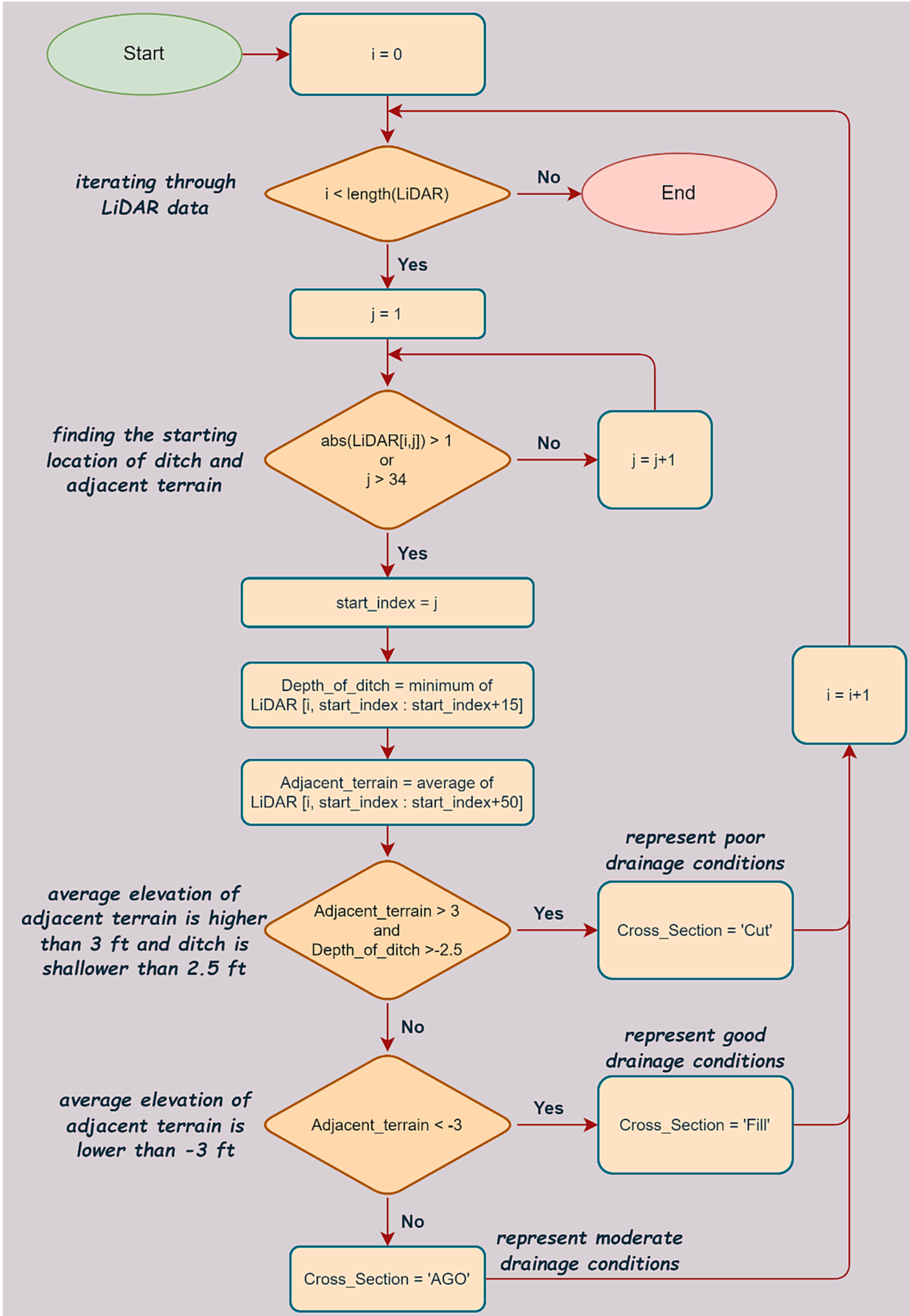

Fig. 5. The flowchart for evaluating drainage and cross section condition from LiDAR data; it should be noted that LiDAR[i, j] is the ground elevation in the i^{th} block and j ft away from the center of track.

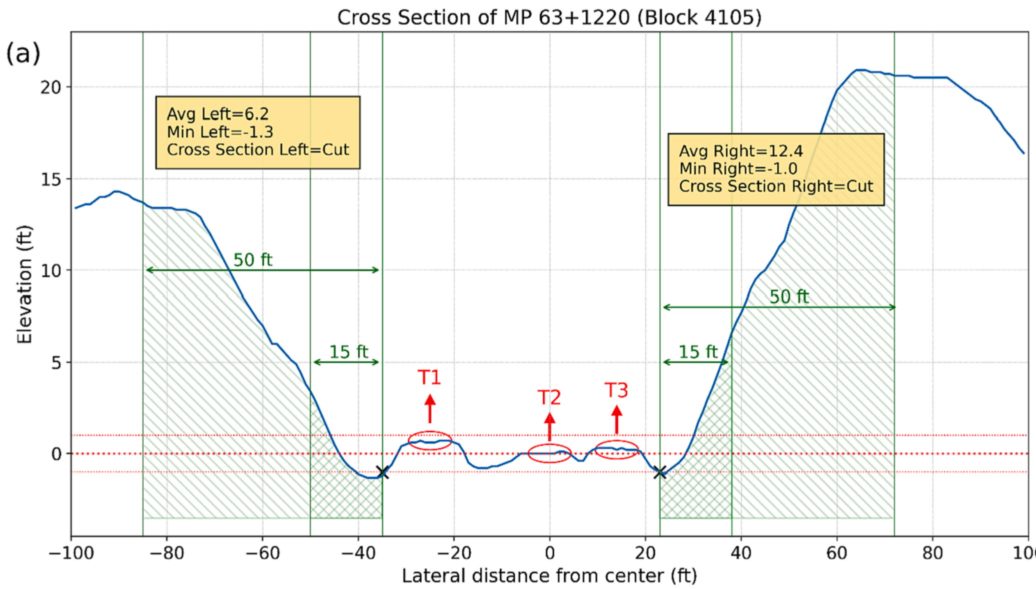

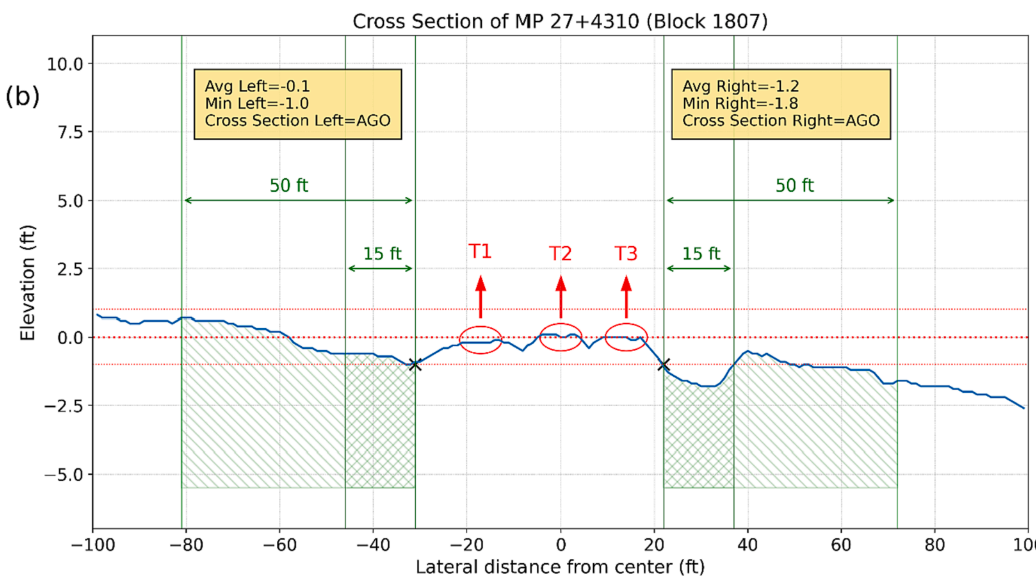

Fig. 6. Applications of the proposed algorithm for determining cross-section and drainage condition of tracks; (a) typical cut cross-section (poor drainage condition) for all three tracks; (b) typical AGO cross section (moderate drainage condition); (c) typical fill cross section (good drainage condition); (d) cut cross-section for right terrain and AGO cross-section for left terrain due to existence of a good ditch.

precipitation will be drained from track, and ditch is not required. On the other hand, the geometry of ditch plays a significant role in the drainage condition of cut or at-grade cross sections. To deal with analyzing large datasets, an algorithm is proposed to automatically evaluate drainage quality. This algorithm copes with the following challenges:

- The distance between adjacent tracks and the distance between ditch and center of track varies along the track. The algorithm should be able to find the exact location of ditch if any ditch exists.
- The algorithm should be able to discriminate ditch from fill cross sections when the relative elevation of adjacent terrain decreases.
- In the case of existing multiple tracks, the further ditch and terrain to a track should not be considered in drainage quality if the distances are too high.

The proposed algorithm in this study solves the mentioned challenges. The flowchart for this algorithm is shown in Fig. 5. The algorithm divides blocks into three categories of cut without good ditch, AGO (At-Grade or Others), and fill cross sections. The category of cut without good ditch represents a poor drainage condition as precipitations will be cumulated close to the track. It is worth noting that for the purpose of brevity, the category of cut without good ditch is referred to simply as "cut" in this paper. On the other hand, fill cross section represents a good drainage condition as it allows for proper drainage of precipitation away from the track. The final category which is AGO represents a moderate drainage condition. To determine the cross-section of track, the starting locations of the adjacent terrain are found, and the average elevation of terrain is compared with the track elevation. In cut cross sections, if the depth of the adjacent ditch is deeper than 2.5 ft (0.76 m) from top of tie (TOT), the cross-section is changed to AGO, which represents moderate drainage condition. In other words, the existence of a good ditch in cut cross sections changes drainage conditions from poor to moderate as it keeps the surface water

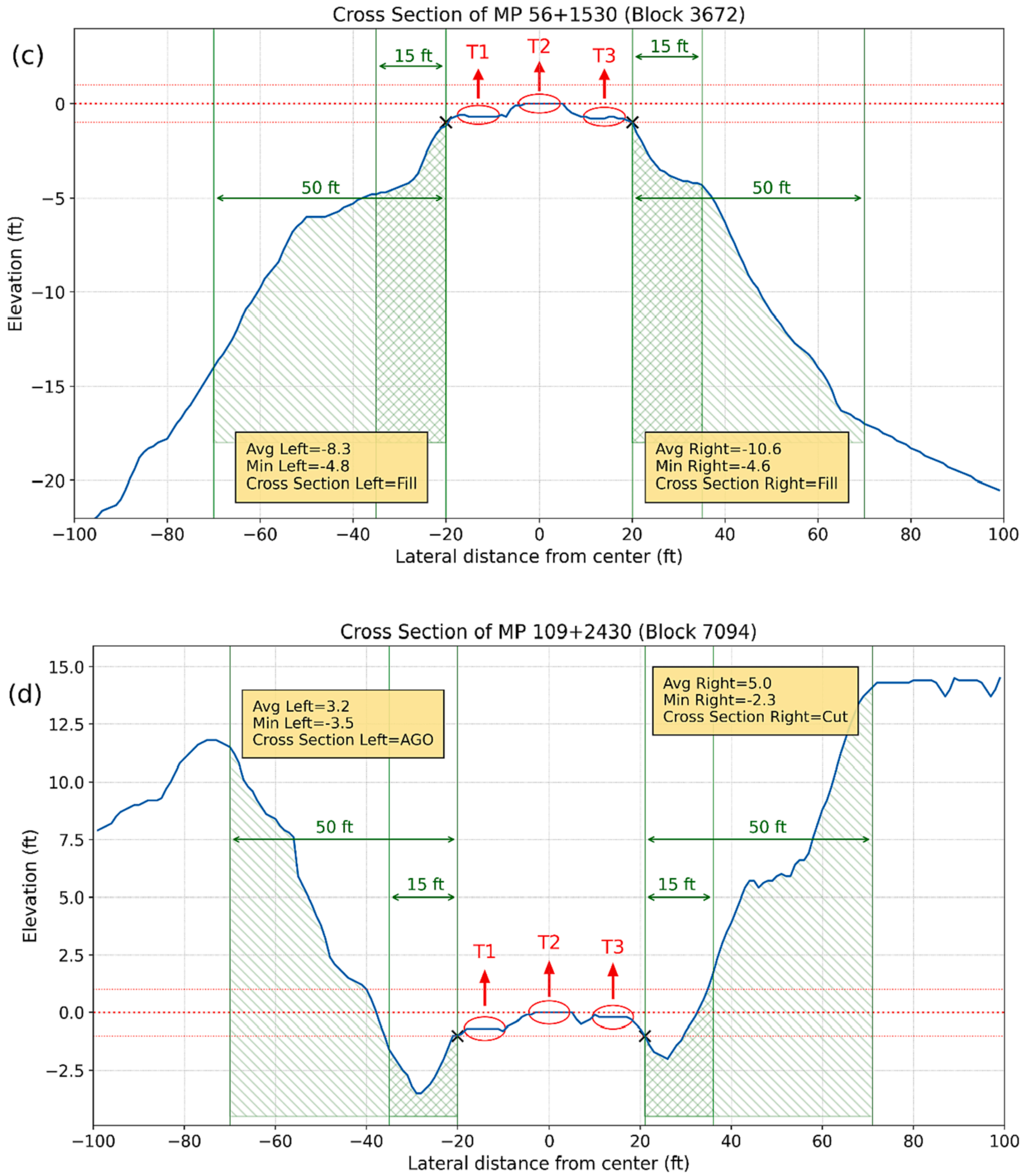

Fig. 6. (*continued*).

away from the track. The 2.5 ft threshold is chosen based on the recommended standard depth of ditch [27].

Fig. 6 shows some applications of the proposed algorithm for evaluating the drainage conditions and cross sections of tracks. The relative elevations has been zeroed on TOT of T2. The black "x" marks show the starting locations of ditches and adjacent terrains, which vary along the track. To find this starting location, the relative elevations are checked from the center of T2 to 35 ft (10.67 m) lateral distance in both side directions. The first location in which the absolute elevation is more than 1 ft (shown by red dotted lines) from the TOT of T2, is marked as the start of ditch and adjacent terrain. The depth of ditch is assessed from the starting point (x mark) up to 15 ft (4.57 m) on each side (double hatched in Fig. 6), while adjacent terrain considers up to 50 ft (15.24 m) on each side (double hatched plus single hatched in Fig. 6). The drainage conditions and cross sections of track are evaluated based on the depth of the ditch and average elevation of adjacent terrain with thresholds of 2.5 (0.76 m) ft for depth of ditch and 3 ft (0.91 m) for average elevation of adjacent terrain. More details are presented in the flowchart of the algorithm (Fig. 5).

Fig. 6 (a) shows a cross-section of track in a cut. Although there are ditches on both sides of the tracks, the ditches are not deep enough (the depths of left and right ditches are 1.3 ft and 1.0 ft, respectively) to keep the water away from the track. Thus, the drainage condition is poor. Fig. 6 (b) shows a typical at-grade cross-section. The drainage condition in this cross-section is moderate as water that falls on adjacent terrain would not cumulate on track. Fig. 6 (c) shows a typical fill cross-section, which represents good drainage conditions. Ditch is not required in fill cross sections as precipitation would flow away from the track on slopes of adjacent terrains. Fig. 6 (d) shows AGO for the left cross-section and cut for the right cross-section. Although the average elevation of the left terrain is 3.2 ft and is higher than the threshold, it was categorized as AGO because the drainage condition is moderate due to the existence of a good ditch. The depth of ditch is 3.5 ft, which is deep enough to keep water adequately away from the track.

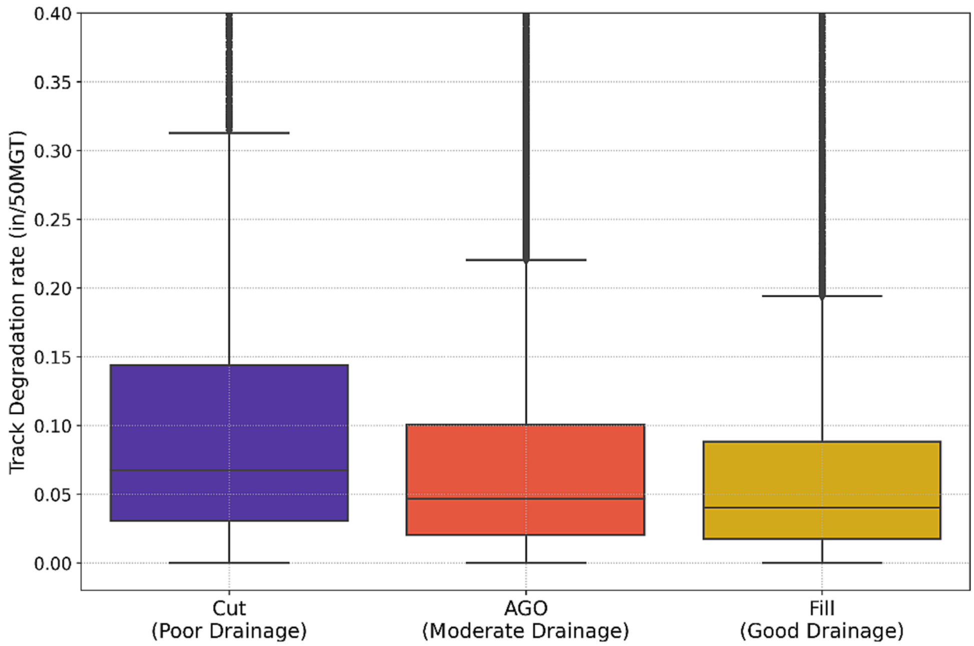

Fig. 7. Box plot of track degradation rate with respect to drainage conditions.

Table 2
Statistical values of track degradation rate in each category.

Name of Category	Count	Min	Median	Max	Standard Deviation	Mean	Skewness	Kurtosis
G1 and Cut	180	0.0025	0.050	0.480	0.0890	0.080	2.39	6.4
G1 and AGO	1,586	0.0007	0.034	0.405	0.0510	0.050	1.92	4.3
G1 and Fill	1,503	0.0008	0.034	0.388	0.0630	0.054	2.52	7.5
G2 and Cut	2,635	0.0015	0.048	0.610	0.0860	0.079	2.22	5.8
G2 and AGO	15,285	0.0009	0.041	0.511	0.0770	0.066	2.52	7.7
G2 and Fill	7,534	0.0009	0.038	0.573	0.0800	0.065	2.61	8.2
G3 and Cut	1,643	0.0059	0.114	1.642	0.2490	0.195	3.11	11.4
G3 and AGO	4,022	0.0021	0.081	1.646	0.2170	0.154	3.43	14.7
G3 and Fill	734	0.0013	0.071	1.110	0.1460	0.120	2.71	9.8
G4 and Cut	530	0.0109	0.179	2.172	0.3790	0.312	2.57	7.0
G4 and AGO	1,067	0.0048	0.162	2.525	0.3940	0.304	2.69	8.5
G4 and Fill	163	0.0141	0.237	1.613	0.2960	0.299	2.16	5.5

Fig. 7 illustrates box plots of track degradation rate with respect to the cross-section and drainage conditions of track. It should be reminded that track degradation rate is calculated using the long period method as it better represents track behavior. The median and 75th percentile of track degradation rate in the cut category is much higher than the other two categories, which indicates detrimental effects of poor drainage conditions on tracks. Although track degradation rate in the fill category is lower than AGO, the difference between these categories is not significant. This fact reveals that moderate drainage condition is enough for reducing the track degradation rate.

4. Stochastic models

Track degradation rate is a function of many variables with an uncertain nature. Measuring all variables that affect track degradation rates is tedious. Even if all variables are measured, there are uncertainties incorporated with them that would be reflected in the track degradation rate. Thus, stochastic and probabilistic models are great approaches for estimating the expected track degradation rate [4]. To propose stochastic models, two variables that highly affect the track degradation rate, namely, subsurface and drainage conditions, are considered. The entire dataset is divided into 12 categories based on these variables. Table 2 presents the statistical values of track degradation rate in each category. The skewness of all categories is positive, which indicates more concentration of datapoints on the left side of the histograms. The counts of two categories, namely, “G1 and Cut” and “G4 and Fill”, are much lower than the other categories, which might be an indicator of rarely occurrence of these two categories in the field. This is presumably due to a better interaction between internal and external drainage in the fill cross sections than cut cross sections. Better interaction between internal and external drainage in fill cross sections will help the water to flow through the ballast matrix resulting in migration of fine particles (fouling) out of ballast layer. However, this interaction in cut cross sections is poor which will help in accumulation of fouling particles in the track. Fig. 8 shows a flowchart diagram that summarizes all steps for stochastic analysis of track degradation rate.

4.1. Fitting probability distributions

To propose stochastic models for track degradation rates, 65 probability distributions are fitted to each category. Probability distributions that fit well with right-skewed datasets (e.g., Lognormal, F-distribution, Dagum, Power Lognormal, Beta prime, Burr, and Johnson SB) are ideal for track degradation rates. The goodness-of-fit tests such as Kolmogorov–Smirnov (K-S), Cramer Von-Mises (CvM), and Chi-Square are conducted for each distribution. The best fitted distribution is chosen based on the Kolmogorov–Smirnov test as it is the most common test for continuous variables [58].

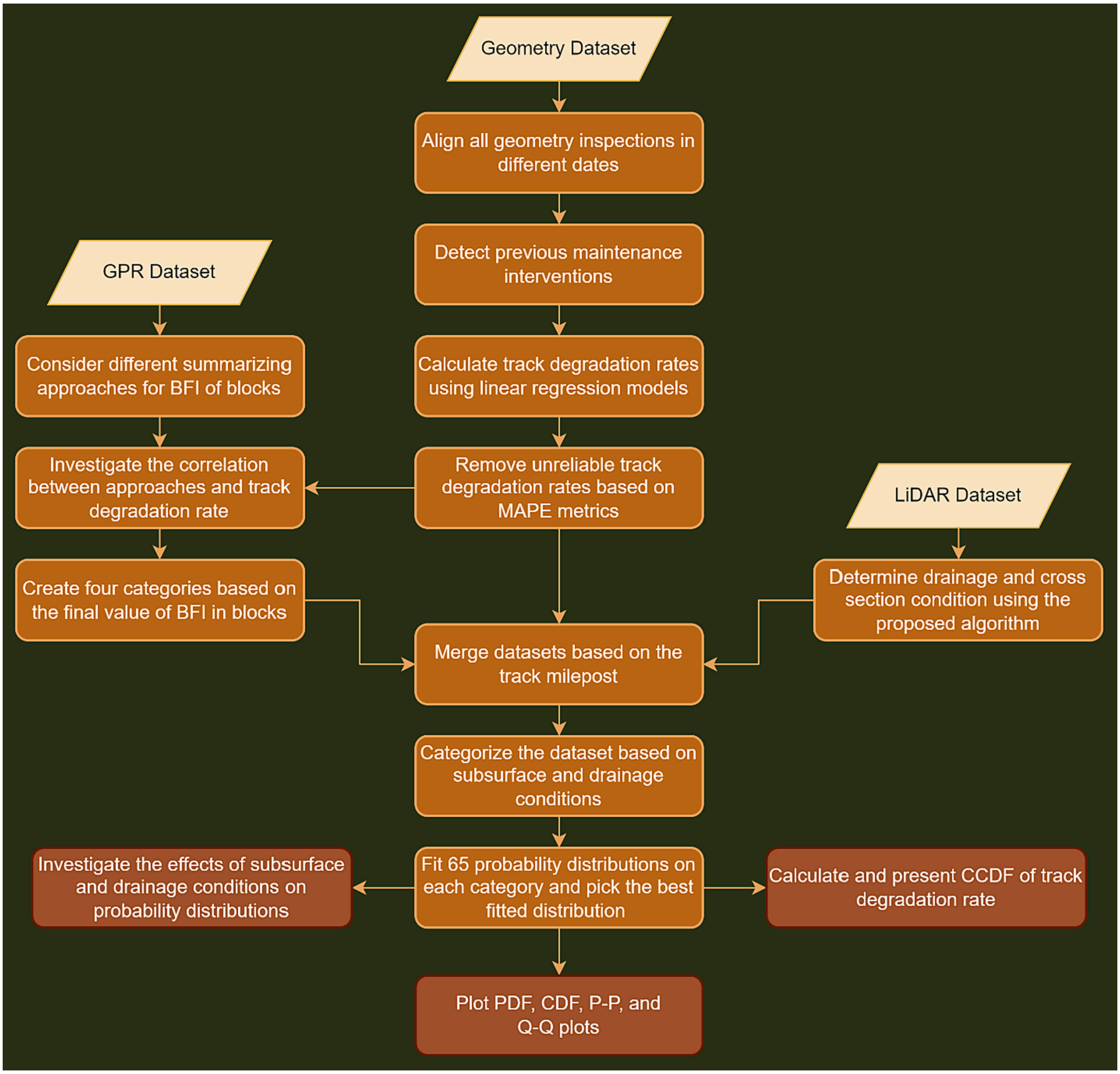

Fig. 8. Flowchart diagram of approach for stochastic analysis of track degradation rate.

Table 3
Goodness-of-fit values and parameters of the best fitted distribution on each category.

Name of Category	Name of Best Fitted Distribution	K-S* Statistic	K-S p-value	CvM** Statistic	CvM p-value	χ2 Statistic	Scale	Location	Shape Parameter1	Shape Parameter2
G1 and Cut	Inverse Weibull	0.0335	0.983	0.0309	0.973	3.74	0.061	−0.02400	1.813	
G1 and AGO	Beta prime	0.0131	0.942	0.0437	0.913	7.35	0.200	0.00013	1.146	5.227
G1 and Fill	F-distribution	0.0157	0.844	0.0674	0.768	4.74	0.041	−0.00001	2.547	6.550
G2 and Cut	Lognormal	0.0133	0.729	0.0895	0.639	16.82	0.052	−0.00319	1.017	
G2 and AGO	Dagum	0.0084	0.226	0.2649	0.170	18.74	0.066	0.00001	1.064	1.857
G2 and Fill	Lognormal	0.0089	0.577	0.1373	0.431	19.88	0.039	−0.00170	1.117	
G3 and Cut	Inverse Gaussian	0.0205	0.511	0.1125	0.527	11.89	0.213	−0.01934	0.829	
G3 and AGO	Power Lognormal	0.0171	0.197	0.2432	0.197	10.79	21.509	−0.00037	47.594	2.558
G3 and Fill	Beta prime	0.0211	0.895	0.0522	0.863	7.13	0.757	0.00002	0.978	7.481
G4 and Cut	Johnson SB	0.0353	0.571	0.1135	0.523	9.18	0.959	−0.00244	1.366	0.889
G4 and AGO	Johnson SB	0.0206	0.793	0.0824	0.678	5.63	0.877	−0.00118	1.094	0.679
G4 and Fill	Johnson SB	0.0416	0.945	0.0296	0.978	2.24	0.658	−0.00236	0.538	0.673

* Kolmogorov–Smirnov.
** Cramer Von-Mises.

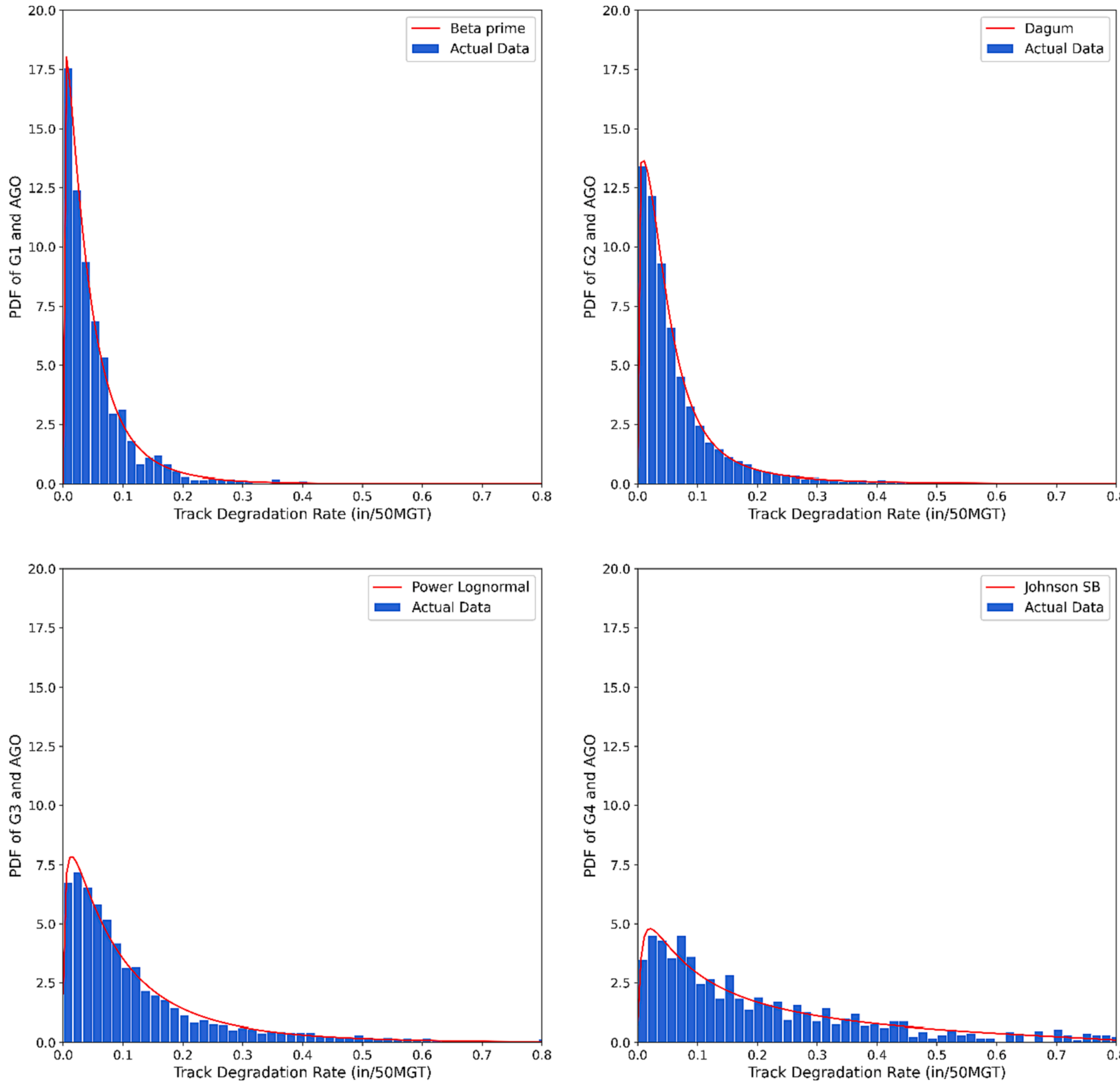

Fig. 9. Histograms and the best fitted distributions of categories from clean ballast (G1) to highly fouled ballast (G4) and AGO cross-section.

Table 3 presents the goodness-of-fit values and parameters of the best-fitted distribution for each category. The null hypothesis in goodness-of-fit is that the dataset follows a specific distribution. Thus, higher p-values in tests represent better fits. The p-value depends on test statistics and critical value, which is a function of number of datapoints and significance level. For a constant critical value, a lower test statistic results in a higher p-value. CvM test is a refined version of K-S test that considers the area between fitted CDF and actual CDF rather than the maximum distance between the curves. Although Chi-Square is usually employed for categorical variables, it can be used for continuous data by dividing the dataset into nonoverlapping bins [59].

Probability distributions are defined by location, scale, and shape parameters. Making a change in location moves the distribution along the x axis, while changing the scale either stretches or squeezes the distribution. In addition to the location and scale, some distributions have shape parameters, which makes them more flexible. These parameters are presented in Table 3 for the best fitted distribution of each category. Appendix Table A is a more detailed version of Table 3, which presents data of five best fitted distributions for each category.

The railway community has two options for estimating expected track degradation rates that are proposed in this paper; (i) employing the presented parameters in Table 3 to recreate probability distributions for a specific category; (ii) referring to Appendix Table B, which presents the CCDF (Complementary Cumulative Distribution Function, which is $1 - CDF$) for each category. The reason for using CCDF rather than CDF is that maintenance scheduling is based on the exceedance probability of a specific track degradation rate.

Fig. 9 displays histograms and the best fitted distributions of categories from clean ballast (G1) to highly fouled ballast (G4) and AGO cross-section. The datapoints are more concentrated on the left side of histograms (i.e., right skewed) regardless of categories. Moving from clean ballast to highly fouled ballast stretches the distribution. The

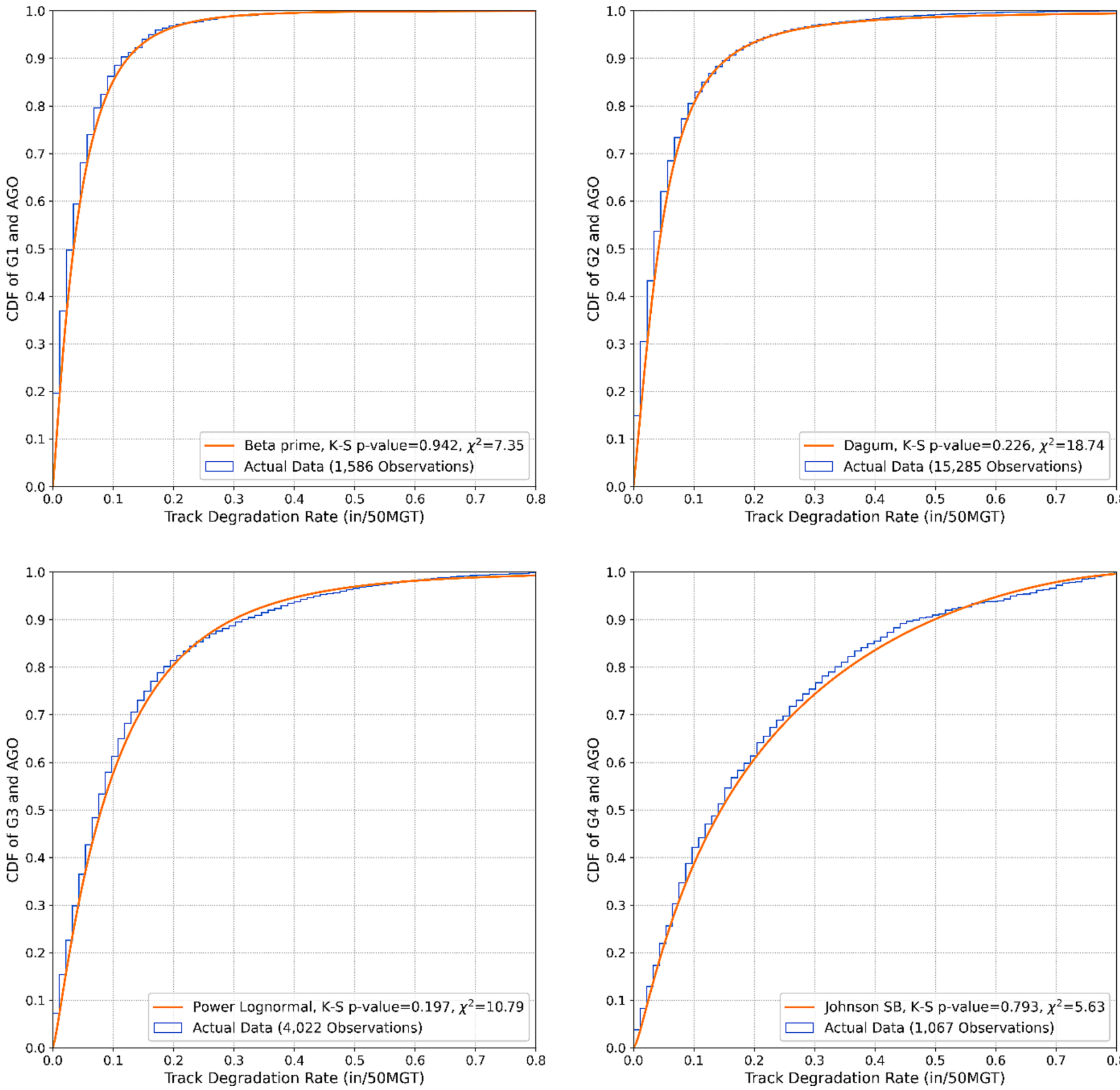

Fig. 10. CDF of actual data and the best fitted distribution of categories from clean ballast (G1) to highly fouled ballast (G4) and AGO cross-section.

probability of having high track degradation rates in G4 is much higher than G1, which indicates the negative effects of fouling on degradation rates.

Fig. 10 shows the CDF of actual data and the best fitted distribution of categories from clean ballast (G1) to highly fouled ballast (G4) and AGO cross-section. Making a comparison between actual data and fitted CDF indicates that probability distributions fitted very well with the data in all four categories. The K-S p-value of G2 and G3 are lower than the other two categories. This is attributed to the very low critical value in these groups. More clearly, the number of observations in G2 and G3 are extremely high, which results in very low critical values for hypothesis testing. Thus, even a small test statistic does not yield a high p-value. To further indicate that the distributions fit the data, Q-Q and P—P plots for G3 (the worst p-value among categories) are presented in Fig. 11. Q-Q and P—P plots are used for visually assessing if the dataset comes from the fitted distribution. As shown in the Q-Q plot, there are only a few datapoints that have small deviations from the red dotted line; however, the majority of datapoints fall exactly on the diameter line, which indicates that the distribution fits the data. The deviation of datapoints in the P—P plot, which compares the empirical CDF with the fitted CDF, is also small. All other categories have higher K-S p-values than “G3 and AGO”. Thus, their theoretical distributions fit even better with the corresponding datasets.

4.2. *Effect of subsurface conditions*

The proposed stochastic models in this paper can be employed for estimating expected track degradation rates, which are required for scheduling geometry maintenance such as tamping. Investigating the effect of subsurface conditions on track degradation rate provides valuable information for making decisions about other types of maintenance such as undercutting. In other words, maintenance operations that clean ballast layer, such as undercutting, are costly. However, they result in a reduction of track degradation rate, which in turn, decreases the need for tamping and increases track safety. By comparing the cost of undercutting and the amount of money that is saved from the reduction of track degradation rates, an informed decision can be made. Fig. 12 shows the effect of subsurface conditions on track degradation rates

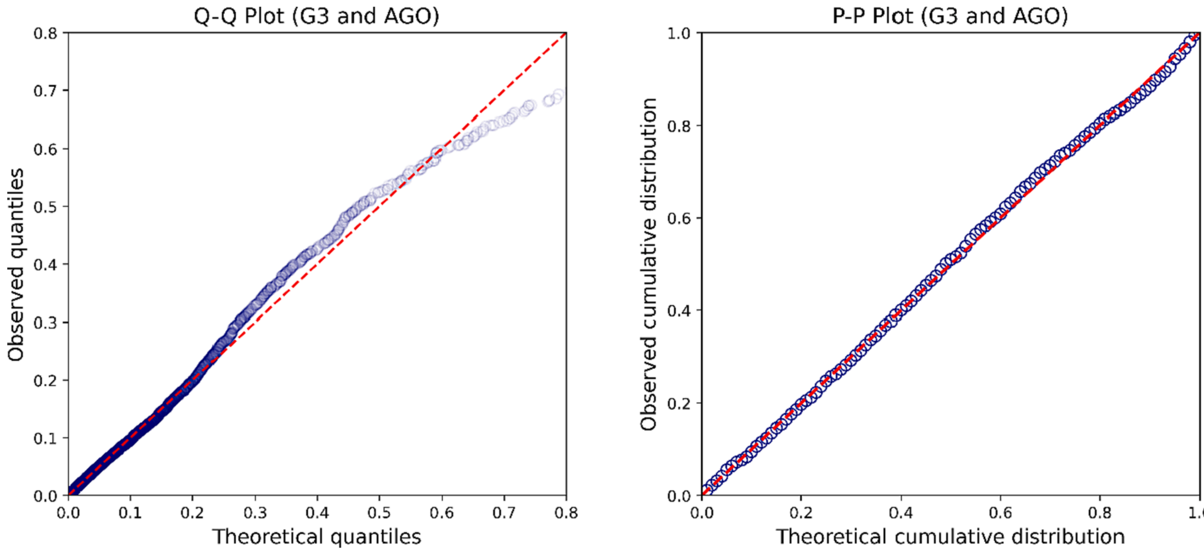

Fig. 11. Q-Q and P—P plots of category "G3 and AGO", which has the lowest K-S p-value among categories.

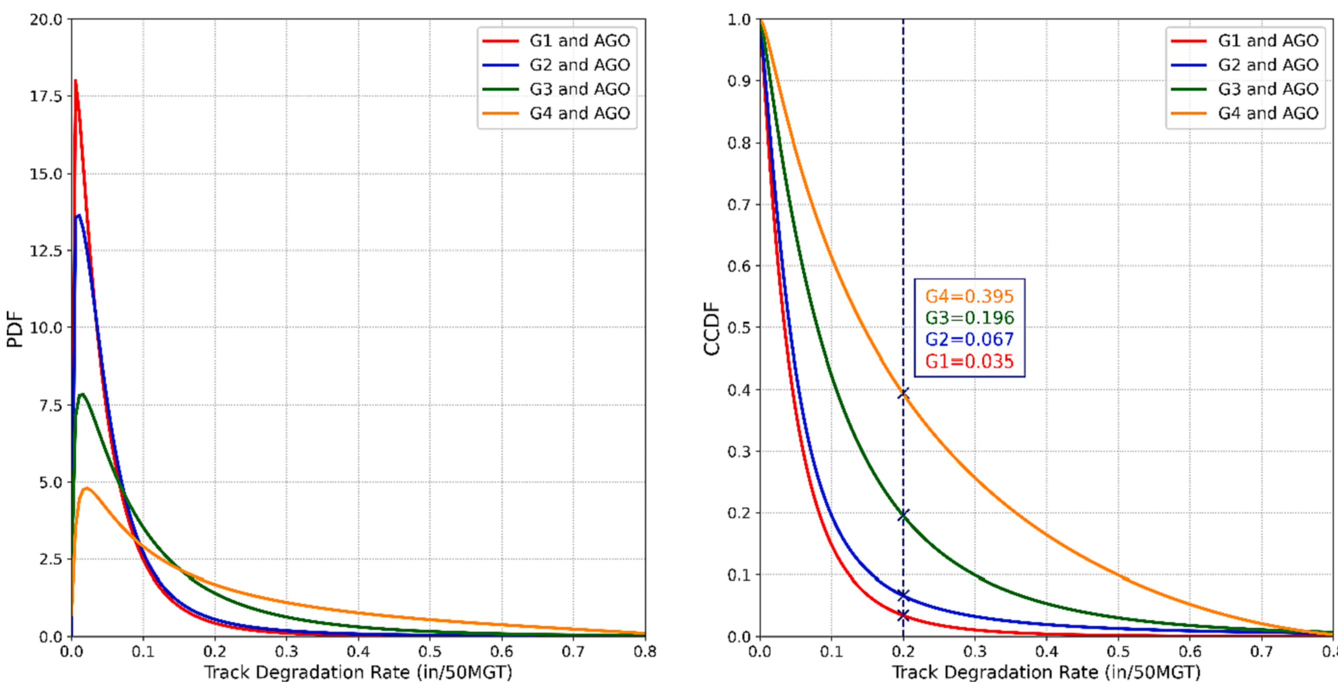

Fig. 12. Effect of subsurface conditions on track degradation rates.

using PDF and CCDF plots. The probability of having high track degradation rates significantly increases by increasing fouling of ballast (i.e., moving from G1 to G4). By considering 0.2 in/50MGT as a threshold, the probability of having high track degradation rates in G4 (i.e., highly fouled ballast) is ten times higher than G1 (i.e., clean ballast). The difference between G2 (BFI between 15 and 25) and G3 (BFI between 25 and 35) is significant, which indicates increasing BFI higher than 25 considerably increases track degradation rates. This finding is consistent with previous laboratory and data analysis studies [5,24,31].

4.3. Effect of drainage and cross-section conditions

Although negative effects of adding water to the track have been studied by laboratory testing [23,25], the effects of drainage conditions on track degradation rates have not been investigated. Analyzing large datasets from the field provides valuable and reliable information for maintaining current or building new ditches to improve drainage conditions. Fig. 13 shows the effect of cut, AGO, and fill cross sections, which represent poor, moderate, and good drainage conditions, respectively. By considering 0.2 in/50MGT as a threshold, the blocks with poor drainage conditions (i.e., cut) are 30% more likely to have high track degradation rates compared to blocks with moderate drainage conditions (i.e., AGO). As explained in Section 3.2, building a ditch with a depth of 2.5 ft (0.76 m) in cut cross sections changes drainage conditions from poor to moderate. Consequently, the probability of having high track degradation rates is reduced by building ditches. As illustrated in the figure, the difference between moderate and good drainage condition is not significant, which indicates moderate drainage condition is enough for keeping precipitation away from the track.

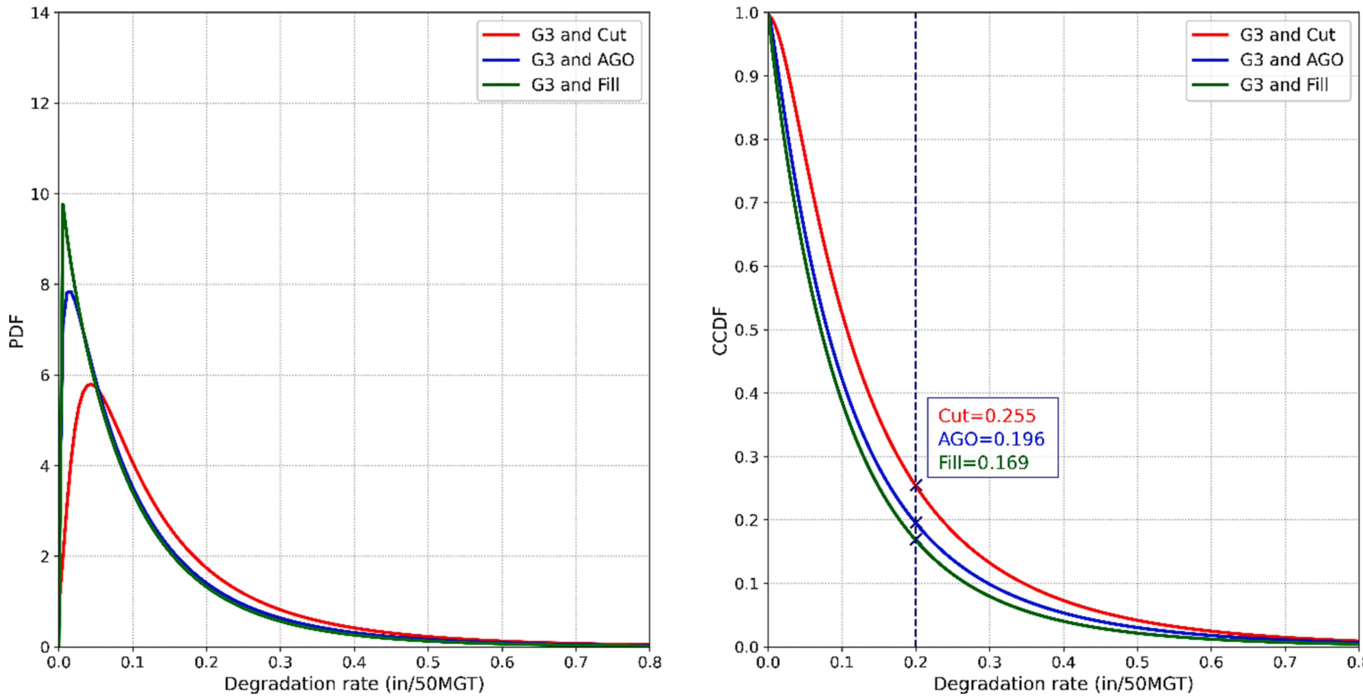

Fig. 13. Effect of drainage and cross-section conditions on track degradation rates.

5. Conclusions

Estimating track degradation rates is required for scheduling preventive maintenance. As track degradation rate is a function of many variables with uncertain nature, stochastic analysis is a great approach for this estimation. In this study, historic geometry data of passenger revenue tracks with a length of 130 miles for the past 11 years are investigated. Stochastic models are proposed for estimating track degradation rates. To increase the estimation accuracy, blocks are divided based on their subsurface and drainage conditions that were derived from GPR and LiDAR data, respectively (Table 2). The conclusions are summarized as follows:

1. Stochastic models are proposed for estimating the expected track degradation rates with respect to subsurface and drainage conditions of track. Results can be used either by rebuilding the probability distributions from the presented parameters or referring to Appendix Table B in the Appendix, which presents CCDF for intervals of track degradation rates.
2. Investigating the effect of subsurface conditions indicated that the probability of having high track degradation rates in highly fouled ballast is 10 times more than in clean ballast, which indicates the detrimental effect of fouling on the track behavior.
3. The difference between track degradation rates of moderately fouled ballast ($15 < \text{BFI} \leq 25$) and fouled ballast ($25 < \text{BFI} \leq 35$) is significant. This indicates that increasing BFI values over 25 results in high track degradation rates.
4. A framework is proposed that can automatically evaluate drainage and cross-section conditions of tracks from LiDAR data.
5. Investigating the effects of drainage and cross-section conditions revealed that blocks with poor drainage conditions are 30% more likely to have high track degradation rates compared to blocks with moderate drainage conditions. Thus, building a ditch with a depth of 2.5 ft (0.76 m) from TOT in cut cross sections is necessary to improve drainage conditions and in turn, reduce track degradation rates.
6. Among the three BFI channels, the center BFI of track shows higher correlations with track degradation rates than shoulders BFI. This could be attributed to the higher stress distributions of train loads in the center of tracks.
7. The long period degradation, which considers previous maintenance interventions, better correlates with BFI than short period degradation. Therefore, it is recommended to employ the long period method in other studies due to better representation of track behavior.

CRediT authorship contribution statement

Saeed Goodarzi: Conceptualization, Methodology, Software, Formal analysis, Investigation, Data curation, Writing – original draft, Writing – review & editing, Visualization. **Hamed F. Kashani:** Conceptualization, Data curation, Funding acquisition, Writing – review & editing. **Anahita Saeedi:** Methodology, Software, Formal analysis, Writing – review & editing. **Jimi Oke:** Formal analysis, Writing – review & editing. **Carlton L. Ho:** Conceptualization, Formal analysis, Writing – review & editing, Supervision, Project administration, Funding acquisition.

Declaration of Competing Interest

The authors declare that they have no known competing financial interests or personal relationships that could have appeared to influence the work reported in this paper.

Data availability

The data that has been used is confidential.

Acknowledgments

This work was supported by the Federal Railroad Administration (FRA) under order No. FR22RPD31000000010. The authors would like to thank Jim Hyslip of HNTB, Aaron Judge of Loram Technologies, Inc, and Steve Chrismer of Amtrak–retired for their support and guidance in helping produce this paper.

Appendix Table A. . Goodness-of-fit values and parameters of five best fitted distributions on each category

Name of Category	Name of Best Fitted Distributions	K-S Statistic	K-S p-value	CvM Statistic	CvM p-value	χ2 Statistic	Scale	Location	Shape Parameter1	Shape Parameter2
G1 and Cut	Inverse Weibull	0.0335	0.983	0.0309	0.973	3.74	0.061	−0.02400	1.813	
	Alpha	0.0344	0.977	0.0375	0.946	5.68	0.173	−0.03954	1.899	
	Lognormal	0.0483	0.770	0.0540	0.852	3.44	0.054	−0.00234	0.981	
	Johnson SU	0.0486	0.765	0.0532	0.857	3.39	0.001	−0.00234	−5.067	1.020
	Exponentiated Weibull	0.0490	0.755	0.0569	0.834	3.56	0.005	−0.00139	9.517	0.417
G1 and AGO	Beta Prime	0.0131	0.942	0.0437	0.913	7.35	0.200	0.00013	1.146	5.227
	F-distribution	0.0131	0.942	0.0437	0.913	7.35	0.044	0.00013	2.293	10.454
	Power Lognormal	0.0145	0.884	0.0531	0.857	4.76	8.302	−0.00009	45.280	2.542
	Exponentiated Weibull	0.0147	0.874	0.0506	0.873	6.89	0.025	0.00008	1.970	0.676
	Burr	0.0250	0.266	0.1822	0.305	20.06	0.065	0.00014	2.157	0.438
G1 and Fill	F-distribution	0.0157	0.844	0.0674	0.768	4.74	0.041	−0.00001	2.547	6.550
	Dagum	0.0168	0.778	0.0365	0.951	2.98	0.055	0.00001	1.057	1.891
	Burr	0.0185	0.673	0.1153	0.515	14.59	0.063	0.00001	2.104	0.450
	Gilbrat	0.0213	0.490	0.1350	0.439	31.71	0.036	−0.00279		
	Power Lognormal	0.0220	0.451	0.1586	0.364	10.68	1.017	−0.00023	12.362	2.119
G2 and Cut	Lognormal	0.0133	0.729	0.0895	0.639	16.82	0.052	−0.00319	1.017	
	Johnson SU	0.0135	0.716	0.0896	0.638	16.99	0.001	−0.00319	−5.211	0.984
	Gilbrat	0.0142	0.655	0.0819	0.681	18.39	0.052	−0.00351		
	Inverse Gaussian	0.0161	0.497	0.1224	0.486	22.28	0.072	−0.00745	1.239	
	Power Lognormal	0.0164	0.473	0.1065	0.554	14.58	0.133	−0.00171	2.502	1.370
G2 and AGO	Dagum	0.0084	0.226	0.2649	0.170	18.74	0.066	0.00001	1.064	1.857
	Beta Prime	0.0110	0.048	0.4382	0.057	29.20	0.128	−0.00002	1.263	3.266
	F-distribution	0.0110	0.048	0.4382	0.057	29.21	0.049	−0.00002	2.526	6.533
	Power Lognormal	0.0148	0.002	1.0337	0.002	66.55	0.970	−0.00039	10.701	2.059
	Exponentiated Weibull	0.0156	0.001	1.1296	0.001	71.28	0.016	−0.00024	3.265	0.532
G2 and Fill	Lognormal	0.0089	0.577	0.1373	0.431	19.88	0.039	−0.00170	1.117	
	Johnson SU	0.0092	0.538	0.1452	0.405	20.43	0.000	−0.00168	−5.253	0.895
	Inverse Gaussian	0.0130	0.154	0.3237	0.116	40.91	0.046	−0.00486	1.611	
	F-distribution	0.0134	0.131	0.2840	0.150	18.50	0.045	−0.00004	2.608	5.447
	Power Lognormal	0.0159	0.042	0.3688	0.087	22.13	0.289	−0.00051	4.950	1.785
G3 and Cut	Inverse Gaussian	0.0205	0.511	0.1125	0.527	11.89	0.213	−0.01934	0.829	
	Exponentiated Weibull	0.0206	0.506	0.0950	0.610	8.23	0.029	−0.00378	5.335	0.548
	Lognormal	0.0222	0.411	0.1266	0.469	13.38	0.117	−0.01001	0.873	
	Johnson SU	0.0225	0.393	0.1317	0.451	13.22	0.001	−0.00998	−5.994	1.145
	Generalized Gamma	0.0237	0.333	0.1751	0.321	9.50	0.031	0.00012	2.618	0.653
G3 and AGO	Power Lognormal	0.0171	0.197	0.2432	0.197	10.79	21.509	−0.00037	47.594	2.558
	Gilbrat	0.0186	0.132	0.3947	0.075	69.42	0.083	−0.00638		
	Beta Prime	0.0187	0.127	0.3480	0.100	17.52	0.459	0.00000	1.162	5.119
	F-distribution	0.0187	0.127	0.3480	0.100	17.52	0.104	0.00000	2.323	10.238
	Exponentiated Weibull	0.0188	0.122	0.3300	0.111	15.46	0.059	−0.00010	2.024	0.672
G3 and Fill	Beta Prime	0.0211	0.895	0.0522	0.863	7.13	0.757	0.00002	0.978	7.481
	Lomax	0.0222	0.856	0.0586	0.823	6.81	0.707	0.00002	7.166	
	Burr	0.0231	0.821	0.0645	0.786	9.82	0.144	0.00002	2.068	0.416
	F-distribution	0.0281	0.604	0.0703	0.750	10.38	0.096	0.00002	1.926	13.463
	Power Lognormal	0.0304	0.500	0.0738	0.729	6.37	63.231	−0.00026	77.938	2.877
G4 and Cut	Johnson SB	0.0353	0.571	0.1135	0.523	9.18	0.959	−0.00244	1.366	0.889
	Generalized Exponential	0.0359	0.547	0.1223	0.486	6.62	0.232	0.00473	0.255	1.133
	Power Lognormal	0.0372	0.502	0.1243	0.479	7.40	45.354	0.00069	135.999	2.184
	Inverse Gaussian	0.0377	0.483	0.0986	0.592	5.69	0.462	−0.03675	0.539	
	Lognormal	0.0395	0.424	0.1183	0.502	7.44	0.185	−0.02410	0.721	
G4 and AGO	Johnson SB	0.0206	0.793	0.0824	0.678	5.63	0.877	−0.00118	1.094	0.679
	Weibull Minimum	0.0211	0.767	0.1157	0.513	13.20	0.206	0.00029	1.015	
	Exponential	0.0229	0.674	0.1296	0.458	18.67	0.205	0.00030		
	Lomax	0.0231	0.664	0.1355	0.437	19.19	3.786	0.00030	1.851	
	Power Lognormal	0.0329	0.236	0.2204	0.231	10.68	157.557	−0.00076	141.538	2.719
G4 and Fill	Johnson SB	0.0416	0.945	0.0296	0.978	2.24	0.658	−0.00236	0.538	0.673
	Exponential Power	0.0464	0.884	0.0611	0.808	4.94	0.390	0.00078	0.981	
	Generalized Gamma	0.0470	0.874	0.0501	0.877	4.66	0.499	0.00078	0.281	3.205
	Exponentiated Weibull	0.0500	0.824	0.0678	0.766	5.88	0.445	0.00078	0.255	3.378
	Chi	0.0533	0.761	0.0844	0.668	6.30	0.281	0.00065	1.049	

Appendix Table B. The exceedance probability (i.e., CCDF) for intervals of track degradation rates in each category

Track Degradation Rate (in/50MGT)	G1 and Cut	G1 and AGO	G1 and Fill	G2 and Cut	G2 and AGO	G2 and Fill	G3 and Cut	G3 and AGO	G3 and Fill	G4 and Cut	G4 and AGO	G4 and Fill
0.00	1.000	1.000	1.000	1.000	1.000	1.000	1.000	1.000	1.000	1.000	1.000	1.000
0.02	0.833	0.673	0.673	0.786	0.735	0.700	0.940	0.857	0.815	0.974	0.922	0.957
0.04	0.596	0.445	0.443	0.571	0.514	0.476	0.832	0.714	0.671	0.914	0.829	0.897
0.06	0.425	0.301	0.303	0.423	0.361	0.341	0.718	0.596	0.555	0.842	0.747	0.837
0.08	0.313	0.208	0.214	0.321	0.261	0.254	0.615	0.500	0.462	0.769	0.676	0.779
0.10	0.239	0.147	0.156	0.249	0.195	0.195	0.526	0.422	0.386	0.699	0.614	0.726
0.12	0.188	0.106	0.117	0.198	0.150	0.154	0.451	0.359	0.324	0.634	0.559	0.676
0.14	0.152	0.078	0.089	0.159	0.118	0.124	0.389	0.306	0.274	0.574	0.511	0.629
0.16	0.125	0.059	0.070	0.130	0.096	0.101	0.336	0.262	0.232	0.519	0.467	0.584
0.18	0.105	0.044	0.055	0.107	0.079	0.084	0.291	0.226	0.197	0.469	0.428	0.543
0.20	0.089	0.035	0.045	0.090	0.067	0.071	0.255	0.196	0.169	0.423	0.395	0.503
0.22	0.077	0.027	0.037	0.076	0.056	0.060	0.221	0.169	0.144	0.382	0.361	0.466
0.24	0.067	0.021	0.030	0.064	0.048	0.051	0.194	0.147	0.123	0.344	0.331	0.430
0.26	0.059	0.017	0.025	0.055	0.042	0.044	0.170	0.128	0.106	0.309	0.304	0.397
0.28	0.052	0.013	0.021	0.048	0.037	0.038	0.150	0.112	0.092	0.278	0.280	0.364
0.30	0.047	0.011	0.018	0.041	0.033	0.033	0.132	0.099	0.080	0.249	0.257	0.334
0.32	0.042	0.009	0.015	0.036	0.029	0.029	0.117	0.087	0.069	0.223	0.235	0.304
0.34	0.038	0.007	0.013	0.032	0.026	0.026	0.104	0.077	0.060	0.200	0.215	0.276
0.36	0.035	0.006	0.012	0.028	0.024	0.023	0.092	0.068	0.053	0.178	0.197	0.250
0.38	0.032	0.005	0.010	0.025	0.021	0.021	0.082	0.060	0.046	0.158	0.180	0.224
0.40	0.029	0.004	0.009	0.022	0.020	0.018	0.073	0.053	0.040	0.141	0.164	0.199
0.42	0.027	0.004	0.008	0.020	0.018	0.017	0.065	0.048	0.035	0.124	0.149	0.176
0.44	0.025	0.003	0.007	0.017	0.016	0.015	0.058	0.042	0.031	0.110	0.135	0.153
0.46	0.023	0.003	0.006	0.016	0.015	0.013	0.052	0.038	0.028	0.096	0.122	0.132
0.48	0.021	0.002	0.006	0.014	0.014	0.012	0.047	0.034	0.024	0.084	0.110	0.111
0.50	0.020	0.002	0.005	0.013	0.013	0.011	0.042	0.030	0.022	0.073	0.099	0.092
0.52	0.019	0.002	0.004	0.012	0.012	0.010	0.038	0.027	0.019	0.064	0.088	0.074
0.54	0.017	0.001	0.004	0.010	0.011	0.009	0.034	0.025	0.017	0.055	0.078	0.071
0.56	0.016	0.001	0.004	0.010	0.011	0.008	0.030	0.022	0.015	0.047	0.069	0.068
0.58	0.015	0.001	0.003	0.009	0.010	0.008	0.027	0.020	0.014	0.040	0.060	0.065
0.60	0.015	0.001	0.003	0.008	0.009	0.007	0.025	0.018	0.012	0.033	0.052	0.058
0.62	0.014	0.001	0.003	0.007	0.009	0.007	0.022	0.016	0.011	0.028	0.045	0.048
0.64	0.013	0.001	0.003	0.007	0.008	0.006	0.020	0.015	0.010	0.023	0.038	0.041
0.66	0.012	0.001	0.002	0.006	0.008	0.006	0.018	0.013	0.009	0.019	0.032	0.035
0.68	0.012	0.001	0.002	0.006	0.007	0.005	0.016	0.012	0.008	0.015	0.026	0.029
0.70	0.011	0.001	0.002	0.005	0.007	0.005	0.015	0.011	0.007	0.012	0.021	0.026
0.72	0.011	0.000	0.002	0.005	0.007	0.004	0.014	0.010	0.006	0.009	0.016	0.018
0.74	0.010	0.000	0.002	0.004	0.006	0.004	0.012	0.009	0.006	0.007	0.012	0.015
0.76	0.010	0.000	0.002	0.004	0.006	0.004	0.011	0.008	0.005	0.005	0.009	0.012
0.78	0.009	0.000	0.001	0.004	0.006	0.004	0.010	0.008	0.005	0.004	0.006	0.009
0.80	0.009	0.000	0.001	0.004	0.005	0.003	0.009	0.007	0.004	0.002	0.004	0.005

References

[1] Z.A. Bukhsh, A. Saeed, I. Stipanovic, A.G. Doree, Predictive maintenance using tree-based classification techniques: A case of railway switches, Transp. Res. Part C Emerg. Technol. 101 (2019) 35–54.

[2] J. Xie, J. Huang, C. Zeng, S.-H. Jiang, N. Podlich, Systematic literature review on data-driven models for predictive maintenance of railway track: Implications in geotechnical engineering, Geosciences 10 (11) (2020) 425.

[3] P.C.L. Gerum, A. Altay, M. Baykal-Gürsoy, Data-driven predictive maintenance scheduling policies for railways, Transp. Res. Part C Emerg. Technol. 107 (2019) 137–154.

[4] N.O. Attoh-Okine, Big Data and Differential Privacy: Analysis Strategies for Railway Track Engineering, John Wiley & Sons, 2017.

[5] S. Goodarzi, H.F. Kashani, J. Oke, C.L. Ho, Data-driven methods to predict track degradation: A case study, Constr. Build. Mater. 344 (2022), 128166.

[6] L. Design, I. Soleimanmeigouni, A. Ahmadi, A. Nissen, X. Xiao, Prediction of railway track geometry defects : a case study, Struct. Infrastruct. Eng. (2019) 1–15, https://doi.org/10.1080/15732479.2019.1679193.

[7] D. Yurlov, A.M. Zarembski, N. Attoh-Okine, J.W. Palese, H. Thompson, Probabilistic approach for development of track geometry defects as a function of ground penetrating radar measurements, Transp. Infrastruct. Geotechnol. 6 (1) (2019) 1–20.

[8] S. Bressi, J. Santos, M. Losa, Optimization of maintenance strategies for railway track-bed considering probabilistic degradation models and different reliability levels, Reliab. Eng. Syst. Saf. 207 (2021), 107359.

[9] H. Li, et al., Improving rail network velocity: A machine learning approach to predictive maintenance, Transp. Res. Part C Emerg. Technol. 45 (2014) 17–26.

[10] C. Vale, M.L. Simões, Prediction of Railway Track Condition for Preventive Maintenance by Using a Data-Driven Approach, Infrastructures 7 (3) (2022) 34.

[11] A.M. Zarembski, J.W. Palese, N. Attoh-Okine, M. Nguyen, H. Thompson, "Can Track Geometry Degradation be Predicted by GPR, Measured Ballast Condition" (2021).

[12] M. Sedghi, O. Kauppila, B. Bergquist, E. Vanhatalo, M. Kulahci, A Taxonomy of Railway Track Maintenance Planning and Scheduling: A Review and Research Trends, Reliab. Eng. Syst. Saf. (2021), 107827.

[13] S. Sharma, Y. Cui, Q. He, R. Mohammadi, Z. Li, Data-driven optimization of railway maintenance for track geometry, Transp. Res. Part C Emerg. Technol. 90 (2018) 34–58.

[14] I. Cárdenas-Gallo, C. A. Sarmiento, G. A. Morales, M. A. Bolivar, and R. Akhavan-Tabatabaei, "An ensemble classifier to predict track geometry degradation," *Reliab. Eng. Syst. Saf.*, vol. 161, no. May 2017, pp. 53–60, 2017, doi: 10.1016/j.ress.2016.12.012.

[15] H. Khajehei, A. Ahmadi, I. Soleimanmeigouni, M. Haddadzade, A. Nissen, M. J. Latifi Jebelli, Prediction of track geometry degradation using artificial neural network: a case study, Int. J. Rail Transp. (2021) 1–20.

[16] J. Chiachío, M. Chiachío, D. Prescott, J. Andrews, A knowledge-based prognostics framework for railway track geometry degradation, Reliab. Eng. Syst. Saf. 181 (2019) 127–141.

[17] N. Alemazkoor, C.J. Ruppert, H. Meidani, Survival analysis at multiple scales for the modeling of track geometry deterioration, Proc. Inst. Mech. Eng. Part F J. Rail Rapid Transit 232 (3) (2018) 842–850, https://doi.org/10.1177/0954409717695650.

[18] Q. He, H. Li, D. Bhattacharjya, D.P. Parikh, A. Hampapur, Track geometry defect rectification based on track deterioration modelling and derailment risk assessment, J. Oper. Res. Soc. 66 (3) (2015) 392–404.

[19] A.R. Andrade, P.F. Teixeira, Statistical modelling of railway track geometry degradation using Hierarchical Bayesian models, Reliab. Eng. Syst. Saf. 142 (2015) 169–183, https://doi.org/10.1016/j.ress.2015.05.009.

[20] A. M. Zarembski, J. W. Palese, and M. Nguyen, "Forecasting Track Geometry Degradation Using GPR Based Ballast Condition," in *ASME/IEEE Joint Rail Conference*, 2022, vol. 85758, p. V001T01A007.

[21] C. Vale, S.M. Lurdes, Stochastic model for the geometrical rail track degradation process in the Portuguese railway Northern Line, Reliab. Eng. Syst. Saf. 116 (2013) 91–98.
[22] M. Audley, J.D. Andrews, The effects of tamping on railway track geometry degradation, Proc. Inst. Mech. Eng. Part F J. rail rapid transit 227 (4) (2013) 376–391.
[23] H.F. Kashani, J.P. Hyslip, C.L. Ho, Laboratory evaluation of railroad ballast behavior under heavy axle load and high traffic conditions, Transp. Geotech. 11 (2017) 69–81.
[24] H.F. Kashani, C.L. Ho, J.P. Hyslip, Fouling and water content influence on the ballast deformation properties, Constr. Build. Mater. 190 (2018) 881–895.
[25] A.K. Rohrman, H.F. Kashani, C.L. Ho, Effects of natural abrasion on railroad ballast strength and deformation properties, Constr. Build. Mater. 247 (2020), 118315.
[26] J. Hyslip, H.F. Kashani, M. Trosino, Ballast State of Good Repair, Am. Railw. Eng. Maint. W. Assoc. AREMA Annu. Conf. (2017).
[27] D. Li, J. Hyslip, T. Sussmann, S. Chrismer, Railway geotechnics, CRC Press, 2015.
[28] M. Esmaeili, J.A. Zakeri, S.A. Mosayebi, Effect of sand-fouled ballast on train-induced vibration, Int. J. Pavement Eng. 15 (7) (2014) 635–644.
[29] A.R.T. Kian, J.A. Zakeri, J. Sadeghi, Experimental investigation of effects of sand contamination on strain modulus of railway ballast, Geomech. Eng. 14 (6) (2018) 563–570.
[30] M. Esmaeili, M. Paricheh, M.H. Esfahani, Laboratory investigation on the behavior of ballast stabilized with bitumen-cement mortar, Constr. Build. Mater. 245 (2020), 118389.
[31] A.R. TolouKian, J. Sadeghi, J.-A. Zakeri, Large-scale direct shear tests on sand-contaminated ballast, Proc. Inst. Civ. Eng. Eng. 171 (5) (2018) 451–461.
[32] M. Fathali, J. Chalabii, F. Astaraki, M. Esmaeili, A new degradation model for life cycle assessment of railway ballast materials, Constr. Build. Mater. 270 (2021), 121437.
[33] T.R. Sussmann, E.T. Selig, J.P. Hyslip, Railway track condition indicators from ground penetrating radar, NDT e Int. 36 (3) (2003) 157–167.
[34] G.R. Olhoeft, E.T. Selig, Ground-penetrating radar evaluation of railway track substructure conditions, Ninth Internat. Conf. Ground Penetrat. Radar 4758 (2002) 48–53.
[35] J. Sadeghi, M.E. Motieyan-Najar, J.A. Zakeri, B. Yousefi, M. Mollazadeh, Improvement of railway ballast maintenance approach, incorporating ballast geometry and fouling conditions, J. Appl. Geophys. 151 (2018) 263–273.
[36] R. Roberts, I. Al-Audi, E. Tutumluer, and J. Boyle, "Subsurface Evaluation of Railway Track Using Ground Penetrating Radar," 2008.
[37] H.F. Kashani, C.L. Ho, W.P. Clement, C.P. Oden, Evaluating the correlation between the geotechnical index and the electromagnetic properties of fouled ballasted track by a full-scale laboratory model, Transp. Res. Rec. 2545 (1) (2016) 66–78.
[38] L.B. Ciampoli, F. Tosti, M.G. Brancadoro, F. D'Amico, A.M. Alani, A. Benedetto, A spectral analysis of ground-penetrating radar data for the assessment of the railway ballast geometric properties, NDT E Int. 90 (2017) 39–47.
[39] Y. Guo, G. Liu, G. Jing, J. Qu, S. Wang, W. Qiang, Ballast fouling inspection and quantification with ground penetrating radar (GPR), Int. J. Rail Transp. (2022) 1–18.
[40] C. Oden, C. Ho, H. Kashani, Man-Portable Real-Time Ballast Inspection Device Using Ground-Penetrating Radar. Railroad Ballast Testing and Properties, ASTM International, 2018.
[41] M. Silvast, A. Nurmikolu, B. Wiljanen, M. Levomaki, An inspection of railway ballast quality using ground penetrating radar in Finland, Proc. Inst. Mech. Eng. Part F J. Rail Rapid Transit 224 (5) (2010) 345–351.
[42] G. Liu, Z. Peng, G. Jing, S. Wang, Y. Li, Y. Guo, Railway ballast layer inspection with different GPR antennas and frequencies, Transp. Geotech. 36 (2022), 100823.
[43] N. Haala, M. Peter, J. Kremer, G. Hunter, Mobile LiDAR mapping for 3D point cloud collection in urban areas—A performance test, Int. Arch. Photogramm. Remote Sens. Spat. Inf. Sci 37 (2008) 1119–1127.
[44] J. Sadeghi, M.E.M. Najar, J.A. Zakeri, C. Kuttelwascher, Development of railway ballast geometry index using automated measurement system, Measurement 138 (2019) 132–142.
[45] H. Lan, C.D. Martin, C. Zhou, C.H. Lim, Rockfall hazard analysis using LiDAR and spatial modeling, Geomorphology 118 (1–2) (2010) 213–223.
[46] W. Zhangyu, Y. Guizhen, W. Xinkai, L. Haoran, L. Da, A camera and LiDAR data fusion method for railway object detection, IEEE Sens. J. 21 (12) (2021) 13442–13454.
[47] M. Taheri Andani, A. Peterson, J. Munoz, M. Ahmadian, Railway track irregularity and curvature estimation using doppler LIDAR fiber optics, Proc. Inst. Mech. Eng. Part F J. Rail Rapid Transit 232 (1) (2018) 63–72.
[48] A. Sánchez-Rodríguez, M. Soilán, M. Cabaleiro, P. Arias, Automated inspection of railway tunnels' power line using LiDAR point clouds, Remote Sens. 11 (21) (2019) 2567.
[49] L. Gézero, C. Antunes, Automated three-dimensional linear elements extraction from mobile LiDAR point clouds in railway environments, Infrastructures 4 (3) (2019) 46.
[50] M. F. Ariyachandra and I. Brilakis, "Detection of Railway Masts in Air-Borne LiDAR Data," 2020.
[51] M. Arastounia, Automated recognition of railroad infrastructure in rural areas from LiDAR data, Remote Sens. 7 (11) (2015) 14916–14938.
[52] A. M. Zarembski, G. T. Grissom, and T. L. Euston, "Use of ballast inspection technology for the prioritization, planning and management of ballast delivery and placement," 2013.
[53] Federal Railroad Administration, "Track and Rail and Infrastructure Integrity Compliance Manual: Volume II - Chapter 1 &2, Track Safety Standards," 2018.
[54] S. Goodarzi, H.F. Kashani, S. Chrismer, C.L. Ho, Using large datasets for finding the correlation between the rate of track settlement and changes in geometry indices, Transp. Geotech. 31 (2021), 100665.
[55] S.-A. Mosayebi, M. Esmaeili, J.-A. Zakeri, Dynamic train–track interactions and stress distribution patterns in ballasted track layers, J. Transp. Eng. Part B Pavements 146 (1) (2020) 4019042.
[56] M. Naeimi, J.A. Zakeri, M. Esmaeili, M. Shadfar, Influence of uneven rail irregularities on the dynamic response of the railway track using a three-dimensional model of the vehicle–track system, Veh. Syst. Dyn. 53 (1) (2015) 88–111.
[57] J. Sadeghi, Development of railway track geometry indexes based on statistical distribution of geometry data, J. Transp. Eng. 136 (8) (2010) 693–700.
[58] H. Pham, Springer Handbook Of Engineering Statistics, vol. 49, Springer, 2006.
[59] Š. Ivošević, R. Meštrović, N. Kovač, Probabilistic estimates of corrosion rate of fuel tank structures of aging bulk carriers, Int. J. Nav. Archit. Ocean Eng. 11 (1) (2019) 165–177.